UNIVERSITY OF LEEDS

This is a repository copy of *Gain-of-Function Genetic Alterations of G9a Drive Oncogenesis*.

White Rose Research Online URL for this paper:
http://eprints.whiterose.ac.uk/169682/

Version: Accepted Version

Article:
Kato, S, Weng, QY, Insco, ML et al. (20 more authors) (2020) Gain-of-Function Genetic Alterations of G9a Drive Oncogenesis. Cancer Discovery, 10 (7). pp. 980-997. ISSN 2159-8274

https://doi.org/10.1158/2159-8290.cd-19-0532

©2020 American Association for Cancer Research. This is an author produced version of an article published in Cancer Discovery. Uploaded in accordance with the publisher's self-archiving policy.

Reuse
Items deposited in White Rose Research Online are protected by copyright, with all rights reserved unless indicated otherwise. They may be downloaded and/or printed for private study, or other acts as permitted by national copyright laws. The publisher or other rights holders may allow further reproduction and re-use of the full text version. This is indicated by the licence information on the White Rose Research Online record for the item.

Takedown
If you consider content in White Rose Research Online to be in breach of UK law, please notify us by emailing eprints@whiterose.ac.uk including the URL of the record and the reason for the withdrawal request.

White Rose university consortium
Universities of Leeds, Sheffield & York

eprints@whiterose.ac.uk
https://eprints.whiterose.ac.uk/

Novel gain-of-function genetic alterations of G9a drive oncogenesis

Authors: Shinichiro Kato[1], Qing Yu Weng[1], Megan L Insco[2,3], Kevin Y Chen[2,3], Sathya Muralidhar[4], Joanna Poźniak[4], Joey Mark Diaz[4], Yotam Drier[5,6,7], Nhu Nguyen[1], Jennifer A Lo[1], Ellen van Rooijen[2,3], Lajos V Kemeny[1], Yao Zhan[1], Yang Feng[1], Whitney Silkworth[1], C Thomas Powell[1], Brian B Liau[8], Yan Xiong[9], Jian Jin[9], Julia Newton-Bishop[4], Leonard I Zon[2,3], Bradley E Bernstein[5,6,7], David E Fisher[1*]

Affiliations:

[1]Cutaneous Biology Research Center, Department of Dermatology, Massachusetts General Hospital, Harvard Medical School, Charlestown, MA 02129, USA.

[2]Howard Hughes Medical Institute, Chevy Chase, ML 20815, USA.

[3]Stem cell program and Division of Pediatric Hematology/Oncology, Boston Children's Hospital, Dana-Farber Cancer Institute, Harvard Medical School, Boston, MA 02115, USA; Department of Stem Cell and Regenerative Biology, Harvard Stem Cell Institute, Cambridge, MA 02138, USA

[4]Institute of Medical Research at St James's, University of Leeds, Leeds, United Kingdom

22 [5]Center for Cancer Research, Massachusetts General Hospital, Boston, MA
23 02114, USA.

24 [6]Department of Pathology, Massachusetts General Hospital, Harvard Medical
25 School, Boston, MA 02114, USA.

26 [7]Broad Institute of MIT and Harvard, Cambridge, MA 02142, USA.

27 [8]Department of Chemistry and Chemical Biology, Harvard University, Cambridge,
28 MA 02138, USA.

29 [9]Department of Pharmacological Sciences and Department of Oncological
30 Sciences, Icahn School of Medicine at Mount Sinai, New York, NY 10029, USA.

31

32

33 *Correspondence to: dfisher3@mgh.harvard.edu

Abstract

Epigenetic regulators, when genomically altered, may become driver oncogenes that mediate otherwise unexplained pro-oncogenic changes lacking a clear genetic stimulus, such as activation of the WNT/β-catenin pathway in melanoma. This study identifies previously unrecognized recurrent activating mutations in the G9a histone methyltransferase gene, as well as G9a genomic copy gains in ~26% of human melanomas, which collectively drive tumor growth and an immunologically sterile microenvironment beyond melanoma. Furthermore, the WNT pathway is identified as a key tumorigenic target of G9a gain-of-function, via suppression of the WNT antagonist DKK1. Importantly, genetic or pharmacologic suppression of mutated or amplified G9a using multiple *in vitro* and *in vivo* models demonstrate that G9a is a druggable target for therapeutic intervention in melanoma and other cancers harboring G9a genomic aberrations.

Significance

Oncogenic G9a abnormalities drive tumorigenesis and the 'cold' immune microenvironment by activating WNT signaling through DKK1 repression. These results reveal a key druggable mechanism for tumor development and identify strategies to restore 'hot' tumor immune microenvironments.

54 **Introduction**

55 The identification and targeting of genomically altered oncogenic drivers remains
56 a compelling therapeutic strategy for otherwise incurable cancers. Disruption of
57 the epigenetic landscape is a relatively common event in cancer, often due to
58 genetic alterations of epigenetic regulatory genes (1). One epigenetic modifier
59 that undergoes somatic recurrent activating oncogenic mutations is enhancer of
60 zeste homolog 2 (EZH2), which can silence expression of target genes (including
61 tumor suppressors) through H3K27 tri-methylation (2). Recurrent mutations of
62 EZH2 have been observed within its SET domain, which is well conserved
63 across SET domain-containing histone methyltransferases (HMTs) and is
64 essential for their enzymatic activity (3–5). The SET domain-containing HMTs
65 Mixed Lineage Leukemia 1 (MLL1) (6), MLL3 (7), and NSD2 (8) are also targeted
66 by gain-of-function genetic alterations that engender oncogenic properties.

67 Another histone methyl transferase, G9a (gene name Euchromatic
68 Histone lysine MethylTransferase 2, *EHMT2*), encodes a primary SET domain-
69 containing enzyme that can catalyze mono- and di-methylation of histone H3K9
70 in a heterodimeric complex with G9a-like protein (GLP) (9). G9a plays critical
71 roles in multiple developmental processes and cell fate decisions through
72 modulation of H3K9me2 levels (10). Genome-wide analysis suggests that
73 H3K9me2 is functionally linked with transcriptional repression (11). Multiple
74 studies have reported elevated G9a expression in various cancers and
75 suggested functional linkages with malignant behaviors of cancer cells (e.g.,
76 aberrant proliferation, chemoresistance, and metastasis) by silencing tumor

77 suppressors (12) and/or activating survival genes (13) or epithelial-to-
78 mesenchymal transition (EMT) programs (14). In addition, recent functional
79 studies have implicated G9a's oncogenic role in MYC-driven tumorigenesis (15).
80 However, genomic alterations of G9a that could directly trigger oncogenesis have
81 not been previously identified. Here we report the occurrence of recurrent
82 activating mutations within the SET domain of G9a and demonstrate their
83 oncogenic function. We further find that genomic copy gains of G9a are relatively
84 common in melanomas and other malignancies, and they display very similar
85 oncogenic activity *in vitro* and *in vivo*. G9a is found to function through repression
86 of DKK1, a negative regulator of the WNT pathway, an important developmental
87 pathway heavily implicated in numerous malignancies including some in which its
88 overactivity has lacked prior mechanistic explanation.

Results

G9a is recurrently mutated and amplified in melanoma patients.

We interrogated publicly available whole-exome sequencing data for human melanomas and identified 6 cases harboring recurrent *G9a* point mutations at glycine 1069 (Fig.1A): four cases with G1069L and two cases with G1069W (p=8.45e-13). The recurrently mutated site, glycine 1069, resides within the highly conserved SET methyltransferase domain (Fig. 1A and B; Supplementary Fig. S1A and S1B; Supplementary Table S1) and aligns two residues from the corresponding location of activating point mutations in the SET domain of *EZH2* (catalytic site Y641, Fig. 1B) (4,5). Furthermore, analysis of all downloadable copy number datasets from TCGA melanomas using GISTIC revealed a significant copy number gain (q-value=7.65e-17) at the 6p21 locus (chr6: 30,950,307-33,085,850), which encompasses the *G9a* gene (Fig. 1C). Comparable statistically significant amplifications of validated oncogenes known to be recurrently mutated or focally amplified in melanoma, such as *MITF (3p13)* (16), *SETDB1 (1q21)* (17), and *NEDD9 (6p24)* (18), were also observed in the same datasets (Fig. 1C). In this analysis, 25.8% of melanomas in the TCGA datasets harbor 3 or more *G9a* copies (shown in Figure 2A along with data on the functional implications of 3 or more *G9a* copies in the section below on the requirement for G9a in *G9a*-gained melanomas). These observations are consistent with the possibility of a gain of function role for G9a in melanoma.

111 **G9a G1069 mutants complexed with GLP enhance H3K9 methylation levels**
112 **and promote melanoma development.**
113 In order to directly determine the functional effect of the G1069L/W point
114 mutations, we tested the *in vitro* catalytic activity of wild-type G9a and the
115 G1069L and G1069W mutants. In the absence of its binding partner GLP, G9a
116 showed significant catalytic activity on several substrates, but neither G9a
117 G1069L nor G9a G1069W displayed significant activity in the absence of GLP
118 (Fig. 1D). We next co-incubated G9a with GLP, which is reported to
119 synergistically increase catalytic activity (19). The G1069L and G1069W
120 mutations do not affect binding potential of G9a with GLP (Supplementary Fig.
121 S1C). However, in the presence of the GLP binding partner, we found that the
122 G9a G1069L and G1069W mutants enhanced H3K9 methylation to a significantly
123 greater degree than wild type G9a (Fig. 1D; Supplementary Fig. S1D). Along with
124 this functional difference, we found that, in the absence of GLP, the G9a
125 G1069L/W mutants bound to H3K9-monomethylated H3 tail peptides with
126 increased efficiency compared to wild type G9a (Supplementary Fig. S1E). A
127 possible explanation for the functional difference warranting further investigation
128 is that tighter binding of the mutants to H3 peptides impairs binding or proper
129 positioning of methyl donor S-adenosylmethionine in the G9a active site, which
130 can be rectified and enhanced by interaction with GLP.
131 H3K27 methylation was not increased by the G9a G1069L/W mutants
132 compared to wild type G9a (Supplementary Fig. S1D), suggesting that the
133 mutations specifically enhance dimethylation of H3K9 without extending

134 substrate specificity to the target of the related EZH2 enzyme. Consistent with
135 these findings, overexpression of the G9a G1069L/W mutants in the human
136 melanoma cell line UACC62 increased H3K9me2 levels more than
137 overexpression of wild type G9a (Supplementary Fig. S1F and S1G).

138 Next, we sought to investigate a functional relationship between the G9a
139 G1069L/W mutants and melanoma development in established *in vitro* and *in*
140 *vivo* assays. First, we tested the impact of these mutations on immortalized
141 human melanocytes (16) (hereafter termed pMEL*) expressing $NRAS^{Q61R}$. These
142 cells exhibited significantly more anchorage-independent growth after addition of
143 G9a WT or the G1069L or G1069W mutant; however, the effects of the mutants
144 were significantly greater than that of wild type G9a (Fig. 1E and F). Similarly,
145 proliferation of UACC62 melanoma cells was significantly increased by
146 overexpression of G9a and further enhanced by the G1069L and G1069W
147 mutants (Supplementary Fig. S1H). These growth advantages were fully
148 reversed by the G9a/GLP inhibitor UNC0638 (Supplementary Fig. S1I), providing
149 initial evidence that G9a/GLP inhibitors might be effective in targeting G9a
150 mutated melanomas.

151 We also tested the impact of these mutants in a $BRAF^{V600E}$;$p53^{-/-}$
152 zebrafish melanoma model. We used the miniCoopR transgenic system (17) to
153 express the G9a G1069L/W mutants and wild type G9a and found that both
154 mutants significantly accelerated melanoma onset compared with EGFP control
155 (Fig. 1G). Unexpectedly, the role of wild type G9a could not be evaluated in
156 zebrafish melanomas because its overexpression resulted in a developmental

157 deficiency of melanocytes compared with control and G9a mutant-expressing
158 zebrafish (Fig. 1H), a phenotype that might be related to the difference in
159 enzymatic function of wild type G9a vs. the point mutants (see Fig. 1D). Since
160 the G9a plasmids were injected into single cell embryos, one possibility is that
161 developing melanocytes with low levels of endogenous zebrafish G9a and GLP
162 homologs will express an excess of human G9a monomer. In the case of wild
163 type G9a, which has activity as a monomer *in vitro*, the excess monomer may
164 methylate H3 at inappropriate sites and cause aberrant gene repression or
165 induction that impairs development of melanocyte progenitor cells. On the other
166 hand, excess mutant G9a monomer will be inactive in melanocyte progenitor
167 cells in zebrafish embryos if it behaves as it does *in vitro*, allowing melanocyte
168 development to proceed until mutant human G9a/zebrafish GLP dimers exert
169 their tumorigenic effects.

170 Further confirmation of the oncogenic function of G9a was provided by a
171 conventional transformation assay in NIH3T3 cells showing copious focus
172 formation by G9a wild type- and mutant-transduced cells (Supplementary Fig.
173 S1J). Together, the *in vitro* and *in vivo* results suggest that G9a is a novel
174 melanoma oncogene and the G9a recurrent mutations at G1069 could be driver
175 mutations for development of melanoma.

176

177 **G9a is required for melanomagenesis and growth in *G9a*-gained**
178 **melanomas.**

179 Along with recurrent mutations, copy number gains/amplifications may be drivers
180 of tumor development in different malignancies with potential for therapeutic
181 targeting. To interrogate candidate genes within the smallest recurrently
182 amplified amplicon in the 6p21 locus, 287 TCGA melanomas with both RNA-seq
183 and SNP array data were analyzed. Amplification of the 6p21 locus is associated
184 with >1.75-fold increased expression of only 4 out of 119 RefSeq genes within
185 the 6p21 amplicon relative to unamplified melanomas; one of these 4
186 overexpressed genes is *G9a* (Supplementary Fig. S2A). Functional validation
187 using multiple shRNA hairpins for each candidate gene (*CCHCR1*, *G9a*, *ZBTB12*,
188 or *RNF5*) revealed that only knockdown of *G9a* consistently suppressed the
189 growth of 6p21-amplified melanoma cell line Hs944T (Supplementary Fig. S2B-
190 S1D). Moreover, of the 4 candidate genes, only G9a expression correlates
191 significantly with poorer prognosis among TCGA melanoma patients
192 (Supplementary Fig. S2E).

193 Because SNP arrays are only semiquantitative with respect to copy
194 number, we measured *G9a* copy numbers using genomic quantitative PCR in 19
195 melanoma cell lines, including Hs944T cells, which are reported in the Cancer
196 Cell Line Encyclopedia database to carry *G9a* amplification (Supplementary Fig.
197 S3A). All of the *G9a* alleles in the 19 melanoma cell lines we utilized are wild type.
198 G9a protein levels that we determined by Western blotting correlated significantly
199 with copy number (Supplementary Fig. S3B-S3D). Consistently, *G9a* mRNA
200 expression levels in *G9a* copy number-gained and -amplified melanomas are
201 significantly higher than that in *G9a* diploid melanomas in the TCGA melanoma

202 dataset (Supplementary Fig. S3E). Important for the functional assessment of
203 G9a activity, western blot analyses indicated that 4 melanoma cell lines with 3 or
204 more copies of *G9a* contained significantly higher overall H3K9me2 levels
205 compared with *G9a*-unamplified melanoma cell lines or primary human
206 melanocytes (Fig. 2B; Supplementary Fig. S3F). Importantly, *G9a* knockdown
207 selectively suppressed proliferation (Fig. 2C) and anchorage-independent growth
208 (Supplementary Fig. S3, G and H) of the *G9a*-gained or -amplified melanoma
209 lines. In LOX-IMVI, a G9a WT/diploid melanoma cell line expressing a high level
210 of G9a (Supplementary Fig. S3C), the growth rate was strongly suppressed by
211 longer treatment (7 days) with G9a knockdown, an effect that was not seen in
212 other G9a WT/diploid melanoma cell lines (Supplementary Fig. S3I), suggesting
213 that G9a-high melanoma cells are consistently sensitive to G9a inhibition, but the
214 molecular kinetics may vary somewhat between *G9a*-diploid melanoma cells with
215 relatively high G9a expression and *G9a*-gained/amplified cells. Conversely, G9a
216 overexpression significantly enhanced anchorage-independent growth of M14, a
217 *G9a*-heterogygous loss melanoma cell line (Supplementary Fig. S3J). Consistent
218 with the genetic findings, *G9a*-gained/H3K9me2-high melanoma cells are highly
219 sensitive to the G9a/GLP inhibitors UNC0638 and BIX01294 compared with *G9a*-
220 unamplified/H3K9me2-low melanoma cells and primary human melanocytes (Fig.
221 2D; Supplementary Table S2). The antiproliferative effect of UNC0638 was
222 strongly associated with accumulation of LC3B-II, an autophagy marker (Fig. 2E),
223 as reported previously (13). Moreover, following treatment with an autophagy
224 inhibitor, bafilomycin A1, accumulation of LC3B-I and -II was strongly promoted

225 in M14 cells overexpressing wild type G9a, and the elevation was further
226 enhanced by expression of the oncogenic G1069L/W mutants (Supplementary
227 Fig. S3K), suggesting that genetic G9a dysregulation confers sensitivity to
228 autophagy inhibitors. Taken together, these data suggest that G9a is required for
229 growth and represents a potential therapeutic target in not only melanomas with
230 G9a point mutations, but also in a larger subset of *G9a* copy number-gained
231 melanomas (about 26% of TCGA melanomas, Fig. 2A).

232 We also tested an additional G9a/GLP inhibitor, UNC0642, with improved
233 potency and pharmacokinetics over UNC0638 *in vivo* (20). This inhibitor strongly
234 suppressed the growth of xenografted tumors of the melanoma cell line K029,
235 which contain 3 copies of the *G9a* gene (Fig. 2F; Supplementary Fig. S4A).
236 UNC0642 treatment was associated with decreased H3K9me2 and increased
237 LC3B levels, at well tolerated drug dosing (Fig. 2G; Supplementary Fig. S4B).
238 UNC0642 induced complete regression of 20-25% of xenografts from *G9a*-
239 gained WM983B and *G9a*-amplified Hs944T melanoma cells (Fig. 2H;
240 Supplementary Fig. S4C and S4D) and significantly extended survival (Fig. 2I;
241 Supplementary Fig. S4E). Similar results were observed in pMEL* cells
242 expressing $BRAF^{V600E}$ and G9a (pMEL*/BRAF/G9a) (16), which exhibit
243 anchorage independent growth (Supplementary Fig. S4F and S4G) similar to
244 pMEL*/NRAS/G9a (refer to Fig. 1D-F), as well as G9a-dependent tumor growth
245 *in vivo* (Supplementary Fig. S4H-S4K). In contrast, the antiproliferative effect of
246 UNC0642 was not seen in *G9a* diploid/wild type melanoma cell line UACC62 *in*
247 *vivo* (Supplementary Fig. S4L).

248

249 **G9a stimulates MITF expression in melanoma through canonical WNT/β-**
250 **catenin signaling.**

251 To elucidate potential mechanisms by which G9a regulates proliferation and
252 melanomagenesis, genome-wide RNA sequencing was performed in *G9a*-
253 amplified Hs944T melanoma cells with and without *G9a* knockdown.
254 Unexpectedly, microphthalmia-associated transcription factor (*MITF*), a master
255 regulator of melanocyte development and survival that is also an amplified or
256 mutated melanoma oncogene (16,21) was downregulated by *G9a* knockdown in
257 the Hs944T cells (Fig. 3A). Consistent with this, several MITF target genes were
258 significantly downregulated in Hs944T cells upon *G9a* knockdown (Fig. 3A;
259 Supplementary Fig. S5A). *MITF* and its target gene *MLANA* were also
260 downregulated consistently by *G9a* knockdown in *G9a*-gained WM983B and
261 K029 melanoma cell lines (Fig. 3B; Supplementary Fig. S5B), but not in multiple
262 *G9a* diploid melanoma lines (Fig. 3B; Supplementary Fig. S5C). Note that we
263 observed unanticipated upregulation of MITF and MLANA upon *G9a* knockdown
264 in some *G9a* diploid or heterozygous loss melanoma cell lines, Mel-juso and M14
265 (Supplementary Fig. S5C), suggesting differential functions of G9a or feedback
266 regulation of G9a by MITF in these melanoma cells. Furthermore, reductions of
267 MITF protein and H3K9me2 levels upon *G9a* knockdown or G9a/GLP inhibition
268 were observed in *G9a*-amplified/gained melanoma cell lines, but not in *G9a*
269 diploid UACC62 cells (Fig. 3C and D; Supplementary Fig. S5D). *G9a* copy
270 number is positively correlated with MITF expression in the TCGA melanoma

271 dataset (Supplementary Fig. S5E). Ectopic MITF was able to partially rescue the
272 growth defect induced by *G9a* knockdown or inhibition in *G9a*-gained and -
273 amplified melanoma cells, but did not affect the growth of *G9a* diploid/wild type
274 melanoma cells with or without *G9a* knockdown (Fig. 3E; Supplementary Fig.
275 S5F-S5H), suggesting that G9a controls survival and growth of *G9a*-
276 gained/amplified melanomas through the stimulation of MITF expression.

277 Accumulating evidence has shown that G9a represses transcription
278 through H3K9 dimethylation (9,11), implying that G9a is likely to elevate MITF
279 levels indirectly in melanomas containing extra *G9a* copies. Several signaling
280 pathways are known to regulate expression of MITF, and genomic dysregulation
281 of these pathways might contribute to development of melanoma (22). To identify
282 G9a-regulated pathways that could contribute to MITF downregulation by *G9a*
283 knockdown, our RNA-seq data were analyzed by gene set enrichment analysis
284 (GSEA). GSEA analysis with the KEGG pathway gene sets revealed enrichment
285 of MITF-related genes in Hs944T-shScr (control) cells, including
286 KEGG_TYROSINE_METABOLISM and KEGG_MELANOGENESIS
287 (Supplementary Table S3). GSEA further revealed that target genes of p300
288 (complexes with CBP) and TCF4 (complexes with LEF1/β-catenin), both of which
289 are key transcriptional co-factors for MITF expression (23,24), are significantly
290 enriched among the genes downregulated by *G9a* knockdown (Supplementary
291 Fig. S6A). This suggests that suppression of TCF/LEF/β-catenin or p300/CBP
292 may be involved in MITF downregulation. Furthermore, WNT/β-catenin-
293 upregulated genes are significantly enriched in Hs944T-shScr cells

294 (Supplementary Fig. S6B). Activation of canonical WNT signaling has been
295 shown to play a vital role in melanocytic development through targeting MITF
296 (24,25). These observations suggest that G9a may activate the canonical WNT
297 pathway by repressing known WNT antagonists. Consistent with this possibility,
298 β-catenin target gene expression, TOPFlash luciferase activity (β-catenin-
299 activated, TCF/LEF-dependent transcription), and nuclear β-catenin expression
300 were all significantly decreased by *G9a* knockdown or G9a/GLP inhibitor
301 UNC0638 in *G9a*-gained and -amplified melanoma cells (Fig. 3F and
302 Supplementary Fig. S6C, and S6D). TOPFlash luciferase activity was not
303 affected by *G9a* knockdown in *G9a* diploid UACC62 cells (Supplementary Fig.
304 S6E). Importantly, MITF downregulation by UNC0638 was fully reversed by
305 ectopic expression of constitutively active β-catenin [β-catenin (S33A)] in *G9a*-
306 gained WM938B cells (Fig. 3G). Basal MITF expression was also upregulated by
307 β-catenin (S33A) in *G9a*-diploid UACC62 cells, but was not affected by G9a/GLP
308 inhibitor UNC0638 (Supplementary Fig. S6F). Therefore, G9a stimulates MITF
309 expression through canonical WNT/β-catenin signaling in *G9a* copy-gained
310 melanoma cells.
311
312 **G9a activates the WNT-MITF axis by repressing WNT antagonist DKK1.**
313 To identify G9a's target gene that can potentially repress the WNT signaling and
314 MITF expression, we comprehensively analyzed our RNA-seq data, including
315 G9a overexpression in pMEL*/BRAF cells and *G9a* knockdown in Hs944T cells.
316 *DKK1* is consistently down- and up-regulated by G9a overexpression in

317 pMEL*/BRAF cells and *G9a* knockdown in Hs944T cells, respectively (Fig. 4A).
318 We then examined a publicly available G9a ChIP-seq data set from colon cancer
319 initiating cells (GSE82131) and found that the putative *DKK1* promoter region is
320 occupied by G9a (Fig. 4B), which we also observed by G9a ChIP-qPCR in
321 Hs944T, but not in UACC62, melanoma cells (Fig. 4C). Furthermore, ChIP-qPCR
322 revealed that G9a inhibition with UNC0638 reduced H3K9 dimethylation at the
323 *DKK1* promoter in Hs944T cells and increased occupancy by phosphorylated-
324 RNApol II (pSer5, marker of active transcription) (Fig. 4D), suggesting that G9a
325 directly represses DKK1 transcription through H3K9me2 histone modification.
326 Consistent with the finding from the genome-wide analysis, expression of DKK1
327 mRNA and protein was induced by either *G9a* knockdown or UNC0638 drug
328 treatment in *G9a*-amplified/gained melanoma cells (Fig. 4E; Supplementary Fig.
329 S6G-S6I). Conversely, DKK1 mRNA and protein expression was repressed,
330 while MITF, its target TRPM1, WNT target CCND1, and pigmentation increased
331 upon G9a overexpression in *G9a*-unamplified melanoma cells (Supplementary
332 Fig. S7A-S7D). G9a overexpression also suppressed DKK1 protein levels in
333 *G9a*-heterogygous loss M14 melanoma cells, along with upregulation of MITF
334 and increased β-catenin activity and H3K9 dimethylation (Supplementary Fig.
335 S7E).

336 To determine whether DKK1 is required for the observed WNT signaling
337 inactivation, MITF downregulation, and growth inhibition in UNC0638-treated
338 *G9a*-gained/amplified melanoma cells, two individual shRNAs targeting *DKK1*
339 were tested. In WM983B and Hs944T cells, UNC0638-induced reductions of

340 nuclear β-catenin and MITF, as well as upregulation of *DKK1* mRNA and
341 downregulation of *MITF* RNA, were fully and largely reversed by shDKK1#2 and
342 shDKK1#3, respectively (Fig. 4F and Supplementary Fig. S7, F and G). In *G9a*
343 diploid/wild type UACC62 cells, on the other hand, both cytosolic and nuclear β-
344 catenin and MITF protein levels were not affected by UNC0638 with or without
345 *DKK1* knockdown (Supplementary Fig. S7G). Moreover, the growth inhibitory
346 effects of UNC0638 on *G9a*-gained WM983B and K029 melanoma cells were
347 correspondingly completely or largely reversed by shDKK1#2 and shDKK1#3,
348 respectively (Fig. 4G), as was upregulation of LC3B-II by UNC0638 (Fig. 4H),
349 however neither of those effects of UNC0638 were observed in UACC62
350 melanoma cells with or without *DKK1* knockdown (Fig. 4G and H). Conversely,
351 overexpression of DKK1 in *G9a*-gained and -amplified melanoma cells was
352 sufficient to decrease active β-catenin and MITF levels as well as growth
353 (Supplementary Fig. S7, H and I). Of note, the G9a G1069L and G1069W
354 mutants have stronger impacts on the repression of DKK1 and the induction of
355 MITF than wild-type G9a (Supplementary Fig. S7, J and K). Taken together,
356 these results suggest that G9a-mediated repression of DKK1 induces activation
357 of the WNT/β-catenin-MITF axis and thereby enhances the growth potential of
358 *G9a* copy number-gained or mutated melanomas.
359
360 **G9a-DKK1-WNT axis is conserved across multiple cancer types beyond**
361 **melanoma.**

362 Almost one third of primary human melanoma specimens have been reported to
363 display nuclear β-catenin accumulation without evidence of somatic mutations
364 within the β-catenin gene (26) or other WNT pathway-related genes (27). *G9a*
365 copy number gains correlate significantly with higher WNT signature scores
366 (p=0.0060, Supplementary Fig. S8A) and occur mutually exclusively with other
367 known genetic alterations within the β-catenin destruction complex, such as loss-
368 of-function mutations or deletions in negative regulators of the WNT pathway
369 (*APC*, *AXIN1*, and *FAT1* (28)) and gain-of-function mutations in β-catenin
370 (Supplementary Fig. S8B). Our study links G9a-mediated epigenetic silencing of
371 DKK1 with aberrant WNT/β-catenin activation in melanoma cells and implies that
372 *G9a* genetic alterations may account for such activation in some melanomas that
373 do not harbor intrinsic WNT pathway somatic mutations that lead more directly to
374 β-catenin accumulation.

375 The WNT signaling pathway has been strongly implicated in
376 tumorigenesis of a wide variety of malignancies beyond melanoma (27),
377 prompting us to examine potential relationships to G9a. We observed the same
378 *G9a-DKK1* inverse correlation in CCLE melanoma and multiple non-melanoma
379 cancer cell panels, including lung, colon, pancreatic, glioma, and sarcoma (Fig.
380 5A). Furthermore, GSEA revealed significant positive correlations between G9a
381 and multiple WNT target gene signatures in melanoma and multiple non-
382 melanoma cancer cell lines (Supplementary Fig. S8C). In particular, all of the
383 CCLE cell line panels that showed inverse *G9a-DKK1* correlations displayed
384 positive correlations with the SANSOM_APC_TARGETS_REQUIRE_MYC gene

385 set (Fig. 5B). Intriguingly, consistent with the strong susceptibility of *G9a*-
386 amplified melanoma to G9a inhibition (Fig. 2), sensitivity to G9a inhibitor BIX-
387 01294 among 325 cancer cell lines in the Cancer Therapeutics Response Portal
388 (http://portals.broadinstitute.org/ctrp.v2.2/), including melanoma, lung cancer,
389 colon cancer, glioma, pancreatic cancer, and sarcoma, correlates significantly
390 with *G9a* mRNA level and copy number (Fig. 5C). Several CCLE non-melanoma
391 cell line panels that did not show a significant correlation between *G9a* and *DKK1*
392 expression still show strong correlations between *G9a* expression and multiple
393 WNT target signatures (Supplementary Fig. S8D), suggesting G9a might activate
394 the WNT signaling pathway through other mechanisms in these cancer types,
395 such as suppression of other WNT antagonists. These bioinformatic analyses
396 suggest that the G9a-WNT signaling axis is highly conserved and G9a potentially
397 contributes to tumorigenesis by activating WNT signaling in a variety of cancers,
398 not limited to *G9a*-amplified or -mutated melanomas.

399 Recently, various molecular and/or genetic alterations in specific cancer
400 cell-intrinsic oncogenic pathways have been reported to affect the degree of T
401 cell infiltration into a given tumor, which correlates with response rate to immune-
402 based therapeutics (29). In melanoma, active β-catenin was implicated in a
403 poorly immunogenic or 'cold' tumor immune microenvironment (e.g., poor
404 recruitment of $CD8^+$ T-cells) and resistance to immune checkpoint (30). On the
405 other hand, another study utilizing a murine engineered melanoma model did not
406 observe the same correlation (31). We therefore examined this question for
407 G9a/WNT activated tumors. We found that *G9a* expression and copy number

408 gain correlate inversely with T-cell signatures [both Spranger T-cell signature
409 (30) and Ayers expanded immune signature (32)] in the TCGA melanoma
410 dataset (Fig. 5D; Supplementary Fig. S8E, S9A and S9B). The correlations of
411 MITF with some of the immune signature genes, in particular Th1
412 cytokines/chemokines (e.g., CXCL9, CXCL10, CXCL11, IFNG and STAT1), are
413 weaker than those of G9a with these genes (Fig. 5D and Supplementary Fig.
414 S9A). We observed some melanoma cases with *G9a* amplification that express
415 low MITF along with low T-cell signatures, suggesting that G9a-induced immune
416 suppression may be mediated by WNT/β-catenin (upstream of MITF), but not by
417 MITF. Also, in non-melanoma cancers, inverse correlations of *G9a* and $CD8^+$ T-
418 cell infiltration are observed (Supplementary Fig. S9C), and are consistent with
419 the functional immune suppressive role of G9a reported in bladder cancer (33).

420 To further interrogate this question with an independent melanoma
421 dataset, 276 primary melanoma specimens obtained from Northern England (the
422 Leeds Melanoma Cohort- LMC) were molecularly annotated (see Methods) and
423 analyzed for *G9a* genomic copy number, *G9a* expression, immune inflammatory
424 signature, and patient outcomes. *G9a* copy number correlated positively with
425 *G9a* gene expression, R=0.4, $P=4.4x10^{-13}$ (Supplementary Fig. S10A). This
426 observation reassured us that further analyses focusing only on copy number
427 alterations were justifiable. Participants whose tumors had high *G9a* copy
428 numbers (highest quartile, N=70) had significantly worse prognoses compared to
429 those with low *G9a* copy number tumors (lowest quartile, N=69): HR=2.5,
430 P=0.001, 95% CI 1.4-3.9 (Supplementary Fig. S10B). Six immunologically

431 different clusters (Consensus Immune Clusters - CICs) were previously reported
432 among the LMC tumors (34), using the immune gene list adapted from Bindea et
433 al. (35). One of these clusters (CIC 4) was a subset of tumors characterized as
434 "cold". CIC4 was depleted of immune signals (imputed T cell, dendritic cell, and
435 cytotoxic cell scores), had significantly increased WNT/β-catenin pathway
436 signaling and the worst survival. On the contrary, CIC2 was identified as immune
437 rich, with reduced WNT/β-catenin signaling and the best prognosis (CIC 2). We
438 therefore tested if tumors with a high *G9a* copy number were associated with
439 these clusters. Indeed, we found that 69% of CIC4 tumors ("cold"/high β-catenin
440 subgroup) had a high *G9a* copy number, a higher percentage than in all other
441 subgroups, Chi^2 p=0.017 (Supplementary Fig. S10C). We also performed a
442 whole transcriptome comparison between tumors with high and low *G9a* copy
443 number, to identify genes/pathways that are differentially expressed between
444 these two tumor groups. Among the pathways that were significantly more highly
445 expressed in *G9a* high tumors, Wnt signaling was agnostically identified as a top
446 correlate (FDR=0.001) (Supplementary Fig. S10D). In a separate whole
447 transcriptome comparison between tumors with high *G9a* copy numbers (highest
448 quartile, N=70) and all of the other tumors in the Leeds cohort (2nd, 3rd, and 4th
449 quartiles, N=206), Wnt signaling was again identified as a top correlate (FDR =
450 2.19×10^{-6}) (Supplementary Table S4).

451 In another publicly available clinical melanoma dataset, higher *G9a* mRNA
452 expression is significantly associated with worse response to anti-CTLA4 therapy
453 (36) (Figure S10E). Also, *G9a* expression shows a tendency to be inversely

454 associated with median survival rate in response to anti-PD1 in melanoma
455 patients in two studies (37,38) (Fig. S10F, G9a high vs. low: 542 days vs 718
456 days). Thus, *G9a* expression can be a predictable biomarker for the response to
457 immune checkpoint blockade. Finally, to examine the functional impact of a
458 G9a/GLP inhibitor on the response to immune checkpoint blockade, we tested
459 combinatorial therapies of UNC0642 with either anti-PD1 or anti-CTLA4 in a
460 syngeneic mouse melanoma model using the G9a wild type D4M.3A.3-UV3 cell
461 line (see Methods). The G9a inhibitor significantly increased complete regression
462 rates to either anti-PD1 or anti-CTLA4 and extended survival in the mouse model
463 (Fig. 5E and F). This result raises the potential that G9a inhibition could improve
464 clinical responses to those immune checkpoint inhibitors in patients with
465 melanoma.

466 **Discussion**

467 The relevance of genetic alterations in epigenetic modulators in cancer has been
468 emphasized by discoveries of high-frequency mutations and copy number
469 changes (39), suggesting the involvement of epigenetic dysregualtion in cancer
470 development. In melanoma, H3K9 methylation/demethylation is likely a key
471 epigenetic modifier of transformation from melanocytes to malignant melanoma
472 (17,40). G9a is a major H3K9me1/2 histone methyltransferase of euchromatin
473 and is often upregulated in different types of cancers. It has also been suggested
474 to mediate aberrant proliferation and metastasis in multiple cancers, however,
475 genomic abnormalities that could activate G9a's oncogenic activity have not
476 previously been identified. Our present study provides evidence that genetic
477 modifications of *G9a*, including mutations within the SET domain and copy
478 number gain/amplification, cause elevated global H3K9me2 levels and
479 accelerate melanomagenesis in conjunction with BRAF(V600E) and
480 NRAS(Q61R) both *in vitro* and *vivo*. These data strongly support the model that
481 *G9a*-G1069 mutations and *G9a* copy number gain are drivers of
482 melanomagenesis.

483 Recurrent gain-of-function mutations within the SET domain have been
484 reported to constitutively activate enzymatic activity alone and/or in epigenetic
485 regulatory complexes. For instance, EZH2 Y641, a key component of the
486 catalytic center for the methyltransferase reaction, has been found to be mutated
487 in diffuse large B cell lymphoma, follicular lymphoma, and melanoma, and
488 promotes oncogenic events in association with high H3K27 trimethylation levels

489 at target genes of polycomb repressive complex 2 (PRC2) (5). In human G9a,
490 the corresponding catalytic tyrosine site, Y1067, is located within the same active
491 site domain as the G1069 residue. G1069 is located adjacent to the histone
492 binding pocket and probably does not physically interact with the histone tail, as
493 shown in a study using structural model analysis of H3K9 HMTs (41). However,
494 replacement of this glycine by a larger hydrophobic non-polar residue (Leu or
495 Trp) that faces the histone-binding pocket is likely to enhance the hydrophobicity
496 of this active site pocket, thereby potentially affecting activity and/or histone
497 binding potential.

498 Due to the change in the histone binding pocket of G9a caused by the
499 G1069 recurrent mutations, the mutant proteins have lost basal catalytic activity,
500 but can induce higher H3K9 methylation than wild type G9a when complexed
501 with binding partner GLP in biochemical assays and in melanoma cells. Similar
502 observations have been made with another SET domain-containing
503 methyltransferase mutant, MLL1 S3865F, the activity of which is also stimulated
504 by its binding partners WDR5/RBBP5/ASH2L (WRA) via an allosteric mechanism
505 (6). In addition, MLL3 Y4884C exhibits higher catalytic activity in the WRA
506 complex than wild type MLL3 complexed with WRA (7). Besides the SET
507 domain-containing methyltransferases, the catalytically inactive DNA
508 methyltransferase-like protein DNMT3L interacts with the catalytic domain of
509 DNMT3A and specifically recruits the DNMT3A-DHMT3L heteromeric complex to
510 unmethylated H3K4, demonstrating that DNMT3L has dual functions of binding
511 the unmethylated histone tail and activating DNA methyltransferases (42). The

512 SET domains of G9a and GLP are required for heterodimer formation (19), and
513 the G9a G1069L/W mutations do not disturb the interaction with GLP
514 (Supplementary Fig. S1C). Therefore, the G9a G1069L/W mutations may induce
515 higher levels of H3K9 methylation due to altered binding potential to histone tails
516 (H3K9me0/1/2 modified histone tails) (Supplementary Fig. S1E) and/or allosteric
517 mechanisms within the GLP-containing complex.

518 In addition to the somatic recurrent mutations of *G9a*, we identified *G9a*
519 copy gains in a significant proportion of TCGA melanomas (3 or more copies of
520 *G9a* in 25.8% of TCGA melanoma patients). We recapitulated this in primary
521 melanoma tumors from the Leeds Melanoma Cohort and showed that copy
522 number is associated with gene expression in that cohort. Furthermore, in an
523 agnostic interrogation of genes differentially expressed in the G9a high vs. G9a
524 low primary tumors, WNT signaling is one of the most strongly upregulated
525 pathways in the G9a high tumors. Our analysis revealed that one or more extra
526 copies of G9a are strongly associated with higher global H3K9me2 levels and
527 dependence on G9a for survival in melanoma cells. Future studies should
528 examine whether elevated H3K9me2 levels predict sensitivity to agents targeting
529 G9a. More recently, frequent *G9a* copy number gains have also been in
530 hepatocellular carcinoma (50% with 3 copies and 10% with 4 or more copies),
531 and HCCs that express high levels of G9a are dependent on its activity (12),
532 suggesting that G9a-targeted therapy could be applicable for patients with non-
533 melanoma cancers.

534 There has been a long-standing question of how the WNT/β-catenin
535 pathway is activated in the many melanomas that lack intrinsic pathway
536 mutations (26). Here we find that G9a-mediated DKK1 silencing activates the
537 WNT/β-catenin-MITF axis to promote melanomagenesis. On the other hand,
538 genetic dysregulation of EZH2 has recently been reported to activate WNT/β-
539 catenin signaling and metastasis by promoting cilium disassembly and
540 subsequent nuclear translocation of β-catenin (43). GISTIC analysis revealed
541 that copy number gain/amplification of *G9a* (chromosome 6p21) and *EZH2*
542 (chromosome 7q34) genomic loci preferentially occur in NRAS- and BRAF-
543 mutated melanoma subsets, respectively (44), suggesting mutual exclusivity of
544 *G9a* and *EZH2* gain/amplification in melanoma patients. Another epigenetic
545 modifier, BRCA1-associated protein-1 (BAP1), is frequently somatically
546 inactivated in cutaneous melanoma, uveal melanoma, renal cell carcinoma and
547 malignant mesothelioma, and highly-penetrant germline *BAP1* mutations
548 predispose to those malignancies (45). As for the reported tumor suppressive
549 mechanism, BAP1 can antagonize EZH2/PRC2 or RING1B (RNF2)/PRC1 in a
550 tissue specific manner (46,47). For instance, while loss of *Bap1* activates intrinsic
551 apoptosis in several mouse cell types (hepatocytes, keratinocytes, fibroblasts,
552 and embryonic stem cells) in an RNF2-dependent fashion, the *Bap1* loss
553 enhances proliferation of melanocytes in association with upregulation of lineage-
554 specific oncogenes MITF and BCL2, independently of RNF2 (48). Therefore,
555 these epigenetic modifiers may share a common endpoint of stimulating WNT
556 signaling and MITF in melanoma.

557 While recent advances in immunotherapy have dramatically improved
558 clinical prognosis of melanoma, substantial proportions of patients exhibit
559 treatment resistance (49). Beyond its oncogenic potential in melanoma, WNT/β-
560 catenin signaling confers multiple aspects of malignant phenotypes, including
561 metastasis (50), acquired resistance to BRAF inhibitor (51), and immune evasion
562 (30). Intriguingly, G9a inhibitor was synergistic with immune checkpoint
563 blockades in a murine melanoma model (Fig. 5E and 5F). Taken together, these
564 studies identify *G9a* as a recurrently mutated and gain-of-function oncogene in
565 melanoma, and also demonstrate its functional role in stimulating WNT-mediated
566 oncogenicity, a behavior that appears to be shared among melanoma and
567 multiple non-melanoma malignancies. Attempts at targeting the WNT pathway
568 pharmacologically have been underway and will be important to develop further.
569 In addition, given the druggability of G9a, this pathway could represent a new
570 therapeutic opportunity both for direct targeting and potentially to enhance
571 immunotherapy efficacy for certain cancers.

572 **Methods**

573

574 **Whole exome sequencing datasets**

575 The mutation annotation files of The Cancer Genome Atlas (TCGA) and 15
576 publicly available whole exome sequencing datasets were downloaded from
577 (https://gdac.broadinstitute.org) (See Supplementary Table S1). Non-
578 synonymous G9a mutations were counted in each dataset and the total cases
579 found in the 16 datasets are summarized in Figure 1A. To evaluate whether the
580 frequency of non-synonymous mutations at G9a G1069 is significantly higher
581 than would be expected if the mutation were neutral (median mutation rate of
582 melanoma:14.4 coding mutations per megabase (39), we computed a one-sided
583 p-value using the dbinom function (Poisson distribution model) in the R statistical
584 software as described previously (52).

585

586 **GISTIC and *G9a* copy number analysis**

587 All downloadable batches (180, 198, 206, 240, 262, 277, 291, 316, 332, 358,
588 388, 393, 408 and 416) of level 3 processed SNP 6.0 array datasets of Skin
589 Cutaneous Melanoma (SKCM) were obtained from the legacy database of The
590 Cancer Genome Atlas (https://tcga-data.nci.nih.gov/docs/publications/tcga/). All
591 of the SNP array data were compiled in one segmentation file and used for
592 further Genomic Identification of Significant Targets in Cancer (GISTIC) analysis.
593 GISTIC analysis was carried out by the GISTIC 2.0 pipeline (GenePattern,
594 https://genepattern.broadinstitute.org/).

595 The putative *G9a* copy number data of 287 TCGA human melanomas were
596 obtained from cBioportal (http://www.cbioportal.org). Based on their analysis, the
597 melanomas were ordered according to the *G9a* copy number (regardless of
598 focality of the *G9a* gain or amplification) and the proportion of melanomas
599 harboring *G9a* copy number gain (3 or more *G9a* copies) and amplification (4 or
600 more copies) were tallied.

601 The *G9a* copy number of melanoma cell lines was determined by genomic
602 DNA quantitative PCR (qPCR). Genomic DNAs of melanoma cells and primary
603 human melanocytes were isolated using DNeasy Blood & Tissue Kit (Qiagen).
604 Primers used for copy number analysis are shown in Supplementary Table S5.
605 The comparative cycle threshold method was used to quantify copy numbers in
606 the samples. Results were normalized to the repetitive transposable element
607 LINE-1 as described previously (16). The relative copy number level was
608 normalized to normal genomic DNA from primary human melanocytes as
609 calibrator.

610

611 **Protein alignment and visualization**

612 Amino acid sequences of SET domains of histone methyltransferases were
613 obtained from NCBI (https://www.ncbi.nlm.nih.gov) and aligned using the
614 ClustalX algorithm. The co-crystal structure of G9a and H3 peptide was obtained
615 from the RCSB Protein Data Bank (PDB: 5jin) and visualized using JSmol
616 (https://www.rcsb.org).

617

618 **Plasmid and mutagenesis**

619 pLenti CMV GFP Blast (659-1) was a gift from Eric Campeau & Paul Kaufman
620 (Addgene plasmid # 17445) and pLenti6-MK1-EHMT2-V5 was a gift from
621 Bernard Futscher (Addgene plasmid # 31113). Mutagenesis was performed
622 using a QuikChange II Site-Directed Mutagenesis kit (Agilent Technologies,
623 Santa Clara, CA) with specific primer pairs (Supplementary Table S5), resulting
624 in mutation of G1069 to L or W in G9a. The resulting mutant sequences were
625 confirmed by conventional Sanger sequencing at the MGH DNA core. The full
626 length human *G9a* wild-type and mutant cDNAs were amplified from the pLenti6-
627 MK1-EHMT2-V5 vector and cloned into pGEX6p1 (GE Healthcare) using the
628 primers indicated in Supplementary Table S5. G9a WT and G1069 mutant
629 cDNAs were also cloned into the pENTR-D/TOPO cloning vector (Thermo
630 Fisher) and subsequently used to establish MiniCoopR vectors for the zebrafish
631 melanoma model as described below (see **Zebrafish melanoma model and**
632 **MiniCoopR system**). GFP and MITF were respectively cloned into the pCW45
633 lentiviral expression vector (Dana-Farber/Harvard Cancer Center DNA Resource
634 Core) as described previously (53). Human *DKK1* cDNA was amplified from
635 discarded human foreskin and cloned into the pCW45 vector. pLenti-hygro-
636 hTERT, pLenti-hygro-CDK4 (R24C), and pLenti-hygro-NRAS^{Q61R} were gifts from
637 Ryo Murakami (Cutaneous Biology Research Center, Massachusetts General
638 Hospital and Harvard Medical School). All pLKO.1-shRNA constructs were
639 obtained from the Molecular Profiling Laboratory (Massachusetts General

640 Hospital Center for Cancer Research). pMD2.G and psPAX2 were gifts from
641 Didier Trono (Addgene plasmid # 12259 and 12260).
642
643 **Lentivirus generation and infection**
644 Lentivirus was generated in Lenti-X^{TM} 293T cells (Clontech, 632180). The Lenti-X
645 cells are transfected using 250 ng pMD2.G, 1250 ng psPAX2, and 1250 ng
646 lentiviral expression vector in the presence with PEI (MW:25K). For infection with
647 lentivirus, 0.1-1 ml of lentivirus-containing media was used in the presence of 8
648 μg/ml Polybrene (Sigma). Selection was performed the day after infection with
649 puromycin (1 μg/ml) or blasticidin (5 μg/ml).
650
651 **Preparation of GST-fused recombinant G9a**
652 GST-tagged G9a (GST-G9a) wild-type and G1069 mutants were expressed in
653 BL21 (DE3) competent cells (Clontech #C2527H) using pGEX6p-G9a constructs.
654 Briefly, the day after transformation with pGEX6p-G9a, a single clone was
655 expanded at 37°C until OD600 reached 0.4-0.6 and further cultured in the
656 presence of 0.5 μM IPTG overnight at room temperature. The BL21 cells were
657 then lysed by sonication in lysis buffer [100 mM NaH_2PO_4, 10 mM Tris-HCl
658 (pH8.0)] supplemented with 1 mM lysozyme, 1 mM PMSF and protease inhibitors
659 (Roche). Soluble proteins were collected by centrifugation (12,000 rpm, 10 min,
660 4°C) and applied to GST spin columns (GST Spin Purification Kit, Thermo
661 Scientific Pierce) according to the manufacture's instruction. The purified protein
662 fractions were subsequently subjected to Amicon® Ultra 50K devices to

663 concentrate GST-fused G9a proteins and replace the buffer with Mg^{2+}- and Ca^{2+}-
664 free PBS. GST-G9a protein concentrations were determined by Bradford protein
665 assay (Pierce) and Coomassie Brilliant Blue (CBB) staining. GST-G9a aliquots
666 were stored at –80°C before use.
667
668 ***In vitro* methyltransferase and pull-down assay**
669 *In vitro* methyltransferase assays were performed using an MTase-Glo™ kit
670 (Promega) according to the manufacturer's instructions. 10 ng/well GST-G9a, 30
671 ng/well histone substrate [unmodified H3 peptide (Abcam, ab7228)], H3K9-
672 modified peptides (Epigentek, R-1024, 1026, and 1028), recombinant human
673 histone H3 (Abcam, ab198757), or human native nucleosome (Thermo Fisher,
674 141057)], and 2 μM S-adenosyl methionine (SAM) were incubated with or without
675 recombinant human GLP (Sigma, SRP0383) in the reaction buffer (50 mM Tris-
676 HCl, pH8.1, 5 mM NaCl, 5 mM MgCl2, 1 mM DTT, 1 mM PMSF, and 1% DMSO)
677 for 1 h at room temperature. After stopping the reaction, the luminescence
678 readout was measured using an EnVision 2104 Multilabel Reader (PerkinElmer).
679 The pull-down assay for recombinant GST-G9a and histone H3 peptides was
680 carried out using a Pull-Down Biotinylated Protein:Protein Interaction Kit (Thermo
681 Fisher) with biotinylated histone H3 (1-21) or H3K9-methylated (me1 or me2) H3
682 tail peptides (Epigentek), according to the manufacturer's protocol. After elution,
683 histone H3-interacting GST-G9a WT and mutant proteins were visualized by
684 immunoblot using anti-GST antibody (ab9085).
685

686 **Protein sample preparation**

687 After the *in vitro* methylation reaction of recombinant H3 protein as described
688 above, an equal volume of 2x Laemmli sample buffer was added to the reaction
689 mixture, which was subsequently used for western blotting and CBB staining.

690 Whole cell lysates were prepared using lysis buffer (25 mM HEPES pH7.7,
691 0.3 M NaCl, 1.5 mM $MgCl_2$, 0.2 mM EDTA, 0.1% Triton X-100) supplemented
692 with protease inhibitors. Nuclear and cytoplasmic proteins were fractionated
693 using NE-PER™ Nuclear and Cytoplasmic Extraction Reagents (Thermo Fisher,
694 78833) according to manufacturer's protocols. Histone proteins were extracted
695 by salt extraction buffer (50 mM Tris-HCl, pH7.6, 0.5M NaCl, 1 % deoxycholic
696 acid, 1 % SDS and 2 mM EDTA) with protease inhibitors. Protein concentrations
697 were quantified by the Bradford protein assay (Thermo Fisher, 23236).

698 Nuclear protein fractions were prepared using a Nuclear Complex Co-IP Kit
699 (Activemotif). Briefly, after extraction of nuclear proteins, protein samples were
700 pre-cleared with control IgG and Pierce Protein A/G UltraLink Resin (Life
701 Technologies, 53133) with 0.25% BSA. Pre-cleared samples were incubated with
702 2 μg of anti-V5 antibody (Abcam, ab27671) or non-specific normal mouse IgG
703 (Santa Cruz Biotechnology, sc-2025) at 4°C overnight and then rotated with
704 Pierce Protein A/G UltraLink Resin at 4°C for 4h. The beads were washed three
705 times and subsequently eluted according to the manufacturer's protocol.

706

707 **Western blotting**

708 Protein samples were resolved by SDS-PAGE and transferred to nitrocellulose
709 membranes. The membranes were blocked in 3% BSA buffer (10 mM Tris-HCl,
710 pH7.4, 150 mM NaCl, 1 mM EDTA, 0.1% Tween-20 and 3% BSA). Primary
711 antibodies used for western blotting were: anti-H3K9me1 (Cell Signaling,
712 #14186), anti-H3K9me2 (Cell Signaling, #4658), anti-H3K9me3 (Wako
713 Diagnostics/Chemicals, 309-34839), anti-H3K27me1 (Cell Signaling, #7693),
714 anti-H3K27me2 (EMD Millipore, #04-821), anti-H3K27me3 (Abcam, ab6002),
715 anti-total H3 (EMD Millipore, 06-755), anti-V5 (Abcam, ab27671), anti-phospho
716 ERK1/2 (Cell Signaling, #4370), anti-ERK1/2 (Cell Signaling, #4695), anti-G9a
717 (Cell Signaling, #3306), anti-GLP (Abcam, ab135487), anti-LC3B (Cell Signaling,
718 #3868), anti-MITF (C5, in-house), anti-active β-catenin (Cell Signaling, #8814), β-
719 catenin (Cell Signaling, #9587), anti-DKK1 (Santa Cruz, sc-374574), anti-β-actin
720 (Santa Cruz, sc-47778), anti-α-tubilin (Sigma Aldrich, T9026), anti-Lamin A/C
721 (Cell Signaling, #4777) and anti-Lamin B (Cell Signaling, #12586). Appropriate
722 secondary antibodies were used in 5% skim milk/TBST buffer. Protein bands
723 were visualized using Western lightning plus ECL (Perkin Elmer) and quantified
724 using ImageJ software.
725
726 **Zebrafish melanoma model and MiniCoopR system**
727 Experiments were performed as published previously (17). In brief, *p53/BRAF/Na*
728 one-cell embryos were injected with 20 ng/μl of control or experimental
729 *MiniCoopR* (MCR) DNA along with tol2 RNA for integration. Control vectors
730 expressed EGFP. Embryos were sorted for melanocyte rescue at 5 days post-

731 fertilization to confirm vector integration. Equal numbers of melanocyte-rescued
732 embryos were grown to adulthood. Twenty fish were raised per tank to control for
733 density effects. Raised zebrafish were scored for the emergence of raised
734 melanoma lesions as published (17).

735 Zebrafish were anesthetized in 0.16 g/L tricaine solution (MS-222) and
736 oriented in an imaging mold (2% agarose in 1 × PBS). Zebrafish were
737 photographed at 10 weeks post-fertilization via brightfield microscopy (Nikon DS-
738 Ri2). Maximum backlight and LED illumination (NII-LED) settings were utilized to
739 distinguish melanocytes from iridophores.

740

741 **DKK1 ELISA**

742 Concentrations of secreted DKK1 in culture supernatant were determined
743 using a Human DKK1 Quantikine ELISA Kit (R&D systems, DKK100) according
744 to the manufacturer's protocols. Briefly, after lentivirus-mediated infections with
745 shG9a- or G9a/V5-expressing vector and proper selections with antibiotics, equal
746 numbers of infected cells were re-plated in 96-well plates. After 72 h of additional
747 culture, the culture supernatants were harvested and subsequently subjected to
748 ELISA. Also, culture supernatants were harvested from DMSO- and UNC0638-
749 treated cells 72 h after treatment. All of the supernatant samples were stored at
750 –80°C after removal of cell debris by centrifugation.

751

752 **Melanoma cell lines and compounds**

753 Hs944T, MeWo, SK-MEL-3 and SK-MEL-28 cells were obtained from ATCC.
754 The WM983B cell line was kindly provided by Meenhard Herlyn (The WISTAR
755 Institute). The K029 cell line was a gift from Dr. Stephen Hodi (DFCI). UACC257,
756 UACC62, MALME3M, LOX-IMVI and M14 cells were obtained from the NCI,
757 Frederick Cancer Division of Cancer Treatment and Diagnosis (DCTD) Tumor
758 Cell Line Repository. SK-MEL-30 and SK-MEL-119 cells were from Memorial
759 Sloan Kettering Cancer Center. MEL-JUSO and MEL-HO cells were from DSMZ.
760 COLO792 cells were purchased from Sigma Aldrich. LB373-MEL cells were from
761 Ludwig Institute of Cancer Research. The VM10 cell lines was established at the
762 Institute of Cancer Research, Medical University of Vienna. UACC257, UACC62
763 and LOX-IMVI melanoma cell lines were cultured in RPMI 1640 supplemented
764 with 1% penicillin/streptomycin/L-glutamine and 9% FBS in a humidified
765 atmosphere of 95% air and 5% CO_2 at 37°C. The other melanoma cell lines were
766 maintained in DMEM with 1% penicillin/streptomycin/L-glutamine and 9% FBS.
767 Human primary neonatal melanocytes were prepared from discarded foreskins
768 and maintained in TIVA medium (F12 medium with 1% penicillin/streptomycin/L-
769 glutamine, 8 % FBS, 50 ng/ml TPA, 225 μM IBMX, 1 μM Na_3VO_4 and 1 μM
770 dbcAMP). Most of the melanoma cell lines have been authenticated by our lab
771 using ATCC's STR profiling service. The following cell lines have not been
772 authenticated because no STR profile information for them was found in any
773 cancer cell line data bank: K029, SK-MEL-119 and VM10.
774 The C57BL/6 syngeneic mouse melanoma cell line D4M.3A was a gift from
775 David Mullins (Dartmouth Geisel School of Medicine), and from it a single cell

776 clone D4M.3A.3 was derived. D4M.3A.3-UV3 cells were generated by
777 sequentially irradiating D4M.3A.3 cells in culture three times with 25 mJ/cm^2 UVB
778 followed by isolation and propagation of single cell clones from the surviving
779 population. The UV3 clone was shown by whole exome sequencing to carry 87
780 mutations/Mb, comparable to somatic mutation rates in human melanomas, and
781 similar expression of PD-L1, PD-1, and MHC class I and II relative to parental
782 D4M.3A.3 cells. D4M.3A.3-UV3 cells were cultured in DMEM with 1%
783 penicillin/streptomycin/L-glutamine and 10% FBS.
784 UNC0638 was purchased from Cayman Chemical (#10734) and
785 reconstituted with DMSO. UNC0642 was provided from Dr. Jian Jin for in vivo
786 experiments. Bafilomycin A1 was purchased from EMD Millipore.
787
788 **Soft agar assay using primary human melanocytes and melanoma cells**
789 Primary human melanocytes were immortalized by simultaneous lentivirus-
790 mediated infections with pLenti-hTERT, pLenti-CDK4 (R24C) and pLenti-p53DD
791 (gifts from Ryo Murakami), followed by hygromycin selection for 3 days and
792 culture for an extended period of time (>30 days) in TIVA media with hygromycin.
793 The resulting polyclonal populations of pMEL/hTERT/CDK4 (R24C) cells were
794 termed pMEL* in this study. The pMEL* cells were infected with pLenti-GFP, -
795 G9a WT, -G9a G1069L or -G9a G1069W. After selection with blasticidin for 1
796 week, these infected pMEL* cells were subsequently infected with pLenti-
797 NRAS^{Q61R} and selected by growth-factor deprivation in F12 medium
798 supplemented with 10% FBS and 1% penicillin/streptomycin/L-glutamine.

799 BRAF^{V600E}-expressing pMEL* cells were established as described previously
800 (16). Also, *G9a*-gained/amplified melanoma cell lines Hs944T and K029 were
801 infected with shG9a hairpins, followed by puromycin selection for 5 days.
802 Following these lentivirus infections, pMEL* and melanoma cells were subjected
803 to a soft agar assay. Briefly, cells (5,000 cells/well in a 24-well plate) were
804 resuspended in 0.1% agarose-containing DMEM with 10% FBS and 1%
805 penicillin/streptomycin/L-glutamine and plated on bottom agar consisting of
806 0.75% agarose in DMEM. 21 days after culture in the soft agar, whole well
807 images were obtained and analyzed for total colony numbers using CellProfiler
808 software (Size: 5-1000, Circularity: 0.2-1).
809
810 **Transformation assay**
811 NIH3T3 cells were plated in 6-cm dishes (2×10^6 cells per well) and cultured until
812 the confluency reached approximately 80-90%. The monolayer cells were then
813 infected with control GFP, wild type G9a, or G1069L/W-mutated G9a lentiviral
814 construct. A day after infection, the lentivirus medium was replaced with fresh
815 regular culture medium and cultured for an additional 10 days. The medium was
816 refreshed every other day. Finally, the cells were fixed with 4% PFA and colonies
817 were visualized by staining with 0.05% crystal violet. Visible macroscopic
818 colonies were counted manually.
819
820 **Cell viability assay**

821 The growth potential of melanoma cells was determined by colony formation
822 assay. Briefly, 72 h after lentivirus infections with shRNAs, equal numbers
823 (10,000 cells/well) of melanoma cells were re-plated in a 12-well plate and further
824 cultured for 7 days. Cell number was estimated by crystal violet staining followed
825 by extraction with 10% acetic acid and measurement at 595 nm using a
826 spectrophotometer (FLUOstar, Omege, BMG LABTECH).

827 The effect of G9a inhibitor UNC0638 on cell viability was evaluated by
828 CellTiter-Glo assay (Promega) and measurement of luminescence using an
829 EnVision 2104 Multilabel Reader (PerkinElmer). Melanoma cells and primary
830 human melanocytes were plated in 96-well black plates (2,000 cells/well)
831 (Thermo Fisher, 07200565) and treated with titrated doses of UNC0638 (0 to 5
832 μM) for 72 h. IC50s of UNC0638 were calculated in GraphPad Prism.

833

834 ***In vivo* xenograft and syngeneic tumor studies**

835 Female hairless SCID mice (crl:SHO-*Prkdc*^{scid} *Hr*^{hr}) aged 5-8 weeks were
836 purchased from Charles River Laboratories. Transformed pMEL* cells
837 expressing BRAF^{V600E} and either GFP or wild type G9a were inoculated
838 subcutaneously at bilateral flank positions (1×10^6 cells in 100 μl PBS(-) per
839 site). Palpable tumor establishment was monitored twice per week and
840 terminated after 8 weeks. Mice harboring palpable pMEL*/BRAF^{V600E}/G9a tumors
841 were subsequently used to test the potency of UNC0642. For longitudinal tumor
842 treatment studies, 5×10^6 K029, WM983B, Hs944T or UACC62 melanoma cells
843 in 100 μl PBS(-) were injected subcutaneously into bilateral flanks. Once tumors

844 reached 50 mm^3, mice were randomly sorted into treatment and control groups
845 ensuring similar initial tumor size. Mice were treated with 2.5 mg/kg UNC0642 or
846 vehicle [10% DMSO/90% PBS(-)] 3 times per week. For syngeneic mouse
847 models, eight-week-old female c57BL/6 mice were obtained from Jackson
848 Laboratory (Bar Harbor, ME). One million melanoma D4M.3A.3-UV3 cells in PBS
849 were inoculated subcutaneously in the right flank. Vehicle or UNC0642 (5 mg/kg)
850 was administrated intraperitoneally daily for the duration of the experiment,
851 starting 6 days after tumor inoculation. Blocking antibodies, anti-PD-1 (a gift from
852 Gordon Freeman, Dana-Farber Cancer Institute) and anti-CTLA-4 (BioXcell,
853 BE0164, clone 9D9), were administrated intraperitoneally on days 7, 9, 11 at a
854 dose of 200 μg per mouse. For survival studies, mice were sacrificed when
855 tumors reached a maximum volume of 1000 mm^3. All studies and procedures
856 involving animal subjects were approved by the Institutional Animal Care and
857 Use Committees (IACUC) of Massachusetts General Hospital and were
858 conducted strictly in accordance with the approved animal handling protocols.
859 Tumor volumes were measured using digital calipers and calculated by the
860 following formula: volume (mm^3) = ($width^2$ x length)/2.
861

862 **Immunohistochemistry**

863 K029 tumors were harvested on Day 17 post-treatment with vehicle or UNC0642,
864 and then were fixed and embedded with formalin and paraffin respectively.
865 Tumor sections were cut at a depth of 5 microns by a microtome, then dried
866 overnight in the oven. Tumor sections were deparaffinized and dehydrated

867 following the standard procedure. Heat-induced antigen retrieval was performed.
868 Immunohistochemical staining was performed by incubation of tumor sections
869 with 1:200 diluted primary antibody for H3K9me2 (Abcam, ab1220) or LC-3B
870 (Cell Signaling, #3868) at 4°C overnight, followed by incubation with 1:2000
871 HRP-linked secondary antibody for 30 minutes at room temperature. Staining
872 results were revealed by applying AEC peroxidase substrate (Vector
873 Laboratories, SK-4200). Hematoxylin-counterstained slides were mounted with
874 coverslips, and staining results were analyzed using a Leica DMR microscope
875 and Nikon NIS-Elements Imaging Software version 4.30.
876
877 **RNA purification and quantitative RT-PCR (qRT-PCR)**
878 RNA was isolated from melanoma cells at indicated time points using the
879 RNeasy Plus Mini Kit (Qiagen). mRNA expression was determined using intron-
880 spanning primers with SYBR FAST qPCR master mix (Kapa Biosystems).
881 Expression was normalized to RPL11. The primers used for qRT-PCR are shown
882 in Supplementary Table S5.
883
884 **Whole transcriptome RNA sequencing (RNA-seq)**
885 Total RNA was extracted from Hs944T melanoma cells 72 h after infection with
886 pLKO.1-shScr or pLKO.1-shG9a#5. All RNA samples were submitted for Quality
887 control (QC), cDNA synthesis, library construction, size selection and NGS
888 sequencing at the Beijing Genomics Institute (BGI, Cambridge, USA). In brief,
889 during the QC steps, an Agilent 2100 Bioanalyzer and ABI StepOnePlus Real-

890 Time PCR System are used in quantification and qualification of the sample
891 library. The multiplexed library was sequenced using an Illumina HiSeq 4000
892 system. Reads were aligned to the reference genome (hg19) by STAR 2.5.2.
893 Reads were counted by HTSeq-0.6.1 using UCSC annotation, as downloaded
894 from the Illumina iGenomes collection. Only reads with mapping score of 10 or
895 more were counted. Differentially expressed genes were detected by DESeq2,
896 using the Wald test.
897
898 **Gene set enrichment analysis (GSEA)**
899 Gene set enrichment analysis was performed using the GSEA module of
900 Genepattern (https://genepattern.broadinstitute.org/). For identifying pathways
901 that are regulated by G9a, our RNA-seq data set was analyzed by GSEA with the
902 Kyoto Encyclopedia of Genes and Genomes (KEGG) pathway gene sets.
903 For correlation between G9a expression and WNT signature gene sets,
904 microarray data of CCLE cancer cell line panels (GSE36133) was analyzed using
905 GSEA. The WNT signature gene set in melanomas was obtained from
906 GSE32907. Briefly, 396 genes that are significantly upregulated by constitutively
907 active β-catenin (β-catenin^{STA}) were identified using the Comparative Marker
908 Selection module (Genepattern) and used as a WNT signature gene set, named
909 WNT_BETA_CATENIN_MELANOMA, in this study. The
910 WNT_BETA_CATENIN_MELANOMA signature gene set was validated in the
911 GSE26656 dataset. Other curated WNT signature gene sets tested were
912 obtained from MSigDB (http://software.broadinstitute.org/gsea/msigdb). G9a

913 expression (probe ID: 207484_s_at) was used as a continuous label and applied
914 to GSEA in accordance with gene set-based permutation and Pearson
915 correlation analysis.

916 For correlation analysis of WNT signatures scores with genetic alterations
917 within WNT pathways, the WNT_BETA_CATENIN_MELANOMA signature
918 scores were computed by single-sample gene set enrichment analysis (ssGSEA)
919 (54), which is able to estimate the degree of coordinated up- and down-regulation
920 of a given gene set, in melanoma cell lines. Genetic profiles (somatic mutations
921 and copy number variations) for all WNT pathway genes were obtained from the
922 CCLE data repository (https://portals.broadinstitute.org/ccle/).

923 Enrichr (http://amp.pharm.mssm.edu/Enrichr/) was used to analyze the
924 enrichment of downregulated genes by *G9a* knockdown (283 genes, log2 fold<-
925 0.585, adjusted p-value<0.05) in annotated genesets (ChEA).

926

927 **TOPFlash/FOPFlash luciferase assay**

928 M50 Super 8x TOPFlash and M51 Super 8x FOPFlash (TOPFlash mutant)
929 plasmids were gifts from Randall Moon (Addgene # 12456 and 12457,
930 respectively). K029 melanoma cells were plated in 24-well plates (5×10^4
931 cells/well) the day before transfection. After shScr- or shG9a-mediated
932 knockdown and subsequent selection with puromycin as described above, the
933 K029 cells were transfected with TOPFlash or FOPFlash vector (0.8 μg/well)
934 along with pRL-SV40 *Renilla* control (0.2 μg/well) using Lipofectamine 2000
935 transfection reagent (Life Technologies). At 72 h, luciferase readings were made

936 using a Dual Luciferase Reporter Assay System (Promega). For testing
937 UNC0638 in the TOPFlash/FOPFlash luciferase assay, 24 h after transfection
938 with the TOPFlash or FOPFlash vector plus pRL-SV40, the transfection medium
939 was replaced with fresh culture medium (10% FBS, 1% penicillin/streptomycin/L-
940 glutamine) containing DMSO or 500 nM UNC0638. 48 h after additional culture in
941 the presence of DMSO or UNC0638, the K029 cells were subjected to the Dual
942 Luciferase Reporter Assay. Firefly luciferase values were normalized to *Renilla*
943 luciferase values. Results reported are the average of three independent
944 experiments done in duplicate.
945
946 **TCGA survival and gene expression analysis**
947 To test the clinical impact of G9a and other candidate genes within the 6p21
948 amplicon, TCGA melanoma patients were ordered according to each candidate
949 gene and survival curves were drawn using OncoLnc (http://www.oncolnc.org).
950 The TCGA RNA-seq data was calculated by RSEM (obtained from cBioportal)
951 and then used for the gene expression analysis in Figure 5D and Supplementary
952 Fig. S9A and S9B.
953
954 **Chromatin immunoprecipitation (ChIP)**
955 ChIPed DNA samples were prepared from 50 million Hs944T cells treated with
956 500 nM UNC0638 or DMSO vehicle for 72 h as described previously (55).
957 Immunoprecipitations were performed with anti-G9a rabbit antibody (Cell
958 Signaling, #3306), anti-H3K9me2 mouse antibody (Abcam, ab1220), anti-

959 phosphor-PolII (Ser5) antibody (Abcam, ab5131), and normal rabbit or mouse
960 IgG (Santa Cruz, sc-2027 or sc-2025) as controls. qPCR assays were performed
961 using primers specific for the human DKK1 putative promoter and the RPL30
962 gene body (see Supplementary Table S5). Ct values of ChIPed DNA samples
963 were normalized to that of 1% Input. The data represent averages of at least
964 three independent experiments.
965
966 **Gene expression analysis in TCGA and Cancer Cell Line Encyclopedia**
967 **(CCLE)**
968 Log-transformed RPKM (Reads Per Kilobase of exon model per Million mapped
969 reads) in melanoma cell lines and TCGA melanoma patients were obtained from
970 CCLE and the Genome Data Analysis Center (GDAC). Gene expression data for
971 88 short-term-cultured melanoma samples were obtained from the Broad
972 Melanoma Portal
973 (http://www.broadinstitute.org/melanoma/branding/browseDataHome.jsf).
974 Correlations between gene expression levels (e.g., G9a vs. DKK1) were
975 calculated by Spearman's rank correlation.
976
977 **BIX-01294 sensitivity and G9a mRNA levels and copy number variations**
978 CCLE gene expression data for G9a was obtained from GSE36133. Copy
979 number data for G9a for all CCLE cell lines were obtained from the Broad
980 Institute website (CCLE_copynumber_byGene_2013-12-03.txt.gz). G9a inhibitor
981 sensitivity was inferred from the area under the curve (AUC) values obtained

982 from the CTRP2.2 database, downloaded from the OCG data portal
983 (https://ocg.cancer.gov/programs/ctd2/data-portal). For the cancer types in which
984 correlations of *G9a* expression with *DKK1* expression and WNT pathway
985 signatures were found as described above, Pearson correlations of the AUC
986 values for BIX-01294 with *G9a* expression and *G9a* copy number values were
987 calculated using Morpheus software
988 (https://software.broadinstitute.org/morpheus).
989

990 **Leeds Melanoma Cohort analysis**

991 Gene expression and copy number alteration data were collected from a cohort
992 of 2184 primary melanoma patients (essentially treatment naive) recruited in the
993 North of England (56,57). Transcriptomic data was generated for 703 tumors and
994 pre-processed as previously described using the Illumina DASL whole genome
995 array (34), accessible from the European Genome-Phenome Archive with
996 accession number EGAS00001002922. The study participants gave informed
997 consent and the study received ethical approval (MREC 1/03/57 and PIAG3-
998 09(d)/2003).

999 Next-Generation Sequencing (NGS)-derived copy number alteration
1000 profiles were generated for 276 tumor samples among the 703 transcriptomic-
1001 profiled tumors as described by Fillia et al. (manuscript under revision). Quality
1002 control of the data was amended afterwards. Briefly, the control germline DNA
1003 sequence data, which were obtained from the Phase 3 data of the 1000
1004 Genomes Project (n=312) (ftp://ftp.1000genomes.ebi.ac.uk/vol1/ftp/phase3/data/)

1005 that matched the experimental setup (Illumina platform, low coverage, paired end
1006 library layout) was used. In order to create bins or windows of size 10k across
1007 the genome, *bamwindow* (https://github.com/alastair-droop/bamwindow) was
1008 utilized. Blacklisted regions (those for which sequence data were unreliable)
1009 were identified and masked. Highly variable regions in the genome were
1010 identified using the QDNASeq package in R and were added to the blacklist. This
1011 pipeline empirically identified highly variable regions including common germline
1012 variations in the genome using the 312 germline controls (58). This step did not
1013 identify any large variation in the germline copy number in the G9a region.
1014 QDNASeq was also used to adjust the read counts from each valid window
1015 based on the interaction of GC content and mappability.

1016 *G9a* copy number data was categorized to identify “High” and “Low” G9a
1017 tumors as first and fourth quartile, respectively. To test the correlations between
1018 *G9a* copy number and *G9a* expression, Spearman’s rank correlation was used.
1019 Survival analysis to assess the association of *G9a* copy number with melanoma-
1020 specific survival (MSS) was performed using a Cox proportional hazards model
1021 and the significance of this model was assessed by the likelihood ratio test. To
1022 test the differences in proportions of *G9a* low and high tumors, among the 6
1023 Consensus Immune Clusters (CICs), chi-squared tests were used. Whole
1024 transcriptome differential gene expression levels between low and high *G9a*
1025 tumors were assessed using Mann-Whitney U tests with the Benjamini-Hochberg
1026 correction for multiple testing (FDR<0.05). Genes identified as significantly
1027 upregulated (z-score<0) or downregulated (z-score>0) were analyzed for

1028 pathway enrichment using Reactome FIViz software; significance of enriched
1029 pathways was denoted by FDR from hypergeometric tests. The volcano plot was
1030 produced using *EnhancedVolcano* package in R.
1031
1032 **Statistical analysis**
1033 The statistical tests indicated in the figure legends were calculated using
1034 GraphPad Prism 7.0 and 8.0. P values < 0.05 were considered statistically
1035 significant.

1036 **Acknowledgements**

1037 The authors thank Dr. Stephen Hodi (Dana-Farber Cancer Institute) for kindly
1038 providing the K029 melanoma cell line. We thank Ryo Murakami (Cutaneous
1039 Biology Research Center, Massachusetts General Hospital and Harvard Medical
1040 School) for the pLenti-hygro-hTERT, hCDK4 (R24C), p53DD, and $NRAS^{Q61R}$
1041 plasmids used for the immortalization of primary human melanocytes. We thank
1042 members of the Fisher laboratory for discussions and suggestions. The results
1043 presented here are fully or partially based upon data generated by the Cancer
1044 Target Discovery and Development (CTD^2) Network
1045 (https://ocg.cancer.gov/programs/ctd2/data-portal) established by the National
1046 Cancer Institute's Office of Cancer Genomics.

1047 **Funding:** This study was supported by grants to D.E.F. from the National
1048 Institutes of Health (5P01 CA163222, 1R01CA222871, 5R01AR072304 and 5R01
1049 AR043369-22), the Melanoma Research Alliance, and the Dr. Miriam and
1050 Sheldon G. Adelson Medical Research Foundation. S.K. acknowledges support
1051 by the Japan Society for the Promotion of Science (JSPS) Postdoctoral
1052 Fellowships for Research Abroad. J.J. acknowledges support by
1053 grants R01HD088626, R01GM122749, and R01CA218600 from the National
1054 Institutes of Health. The Leeds research was funded by Cancer Research UK
1055 C588/A19167, C8216/A6129, and C588/A10721 and NIH CA83115. J.P., J.P,
1056 J.M.D and S.M. were funded by Horizon 2020 Research and Innovation
1057 Programme no. 641458 (MELGEN).

1058 **Author contributions:** S.K., Q.Y.W., L.I.Z., B.E.B., and D.E.F. designed and
1059 conducted the experiments; J.N.B. funded and led the LMC project, recruited the
1060 participants and supervised the LMC bioinformatic analysis; S.K. and Q.Y.W.
1061 performed the majority of the *in vitro* and *in vivo* experiments; Y.D. analyzed
1062 RNA-seq data; S.K., C.T.P. and L.V.K. analyzed copy number and gene
1063 expression data, and performed bioinformatics analyses; M.L.I, K.C. and E.R.
1064 performed zebrafish melanoma experiments and the associated statistical
1065 analyses; S.J. and J.P. analyzed LMC datasets and interpreted the results;
1066 J.M.D. computed copy number data quality control of LMC. Y.Z. performed
1067 immunohistochemistry; F.Y. performed TOPFlash/FOPFlash luciferase assays;
1068 W.S. maintained melanoma cell lines and performed crystal violet assays; B.L.
1069 helped G9a protein model analysis; Y.X. and J.J. synthesized and provided
1070 UNC0642; C.T.P confirmed statistical analyses; S.K., C.T.P., and D.E.F. wrote
1071 most of the manuscript; all authors wrote parts of their responsible experiments
1072 and reviewed and approved the manuscript.

1073 **Competing interests:** S.K., Q.Y.W., and D.E.F. declare that parts of the work
1074 are the subject of a U.S. provisional patent application titled "Treatment of
1075 cancers having alterations within the SWI/SNF chromatin remodeling complex."
1076 Dr. Fisher has a financial interest in Soltego, Inc., a company developing SIK
1077 inhibitors for topical skin darkening treatments that might be used for a broad set
1078 of human applications. Dr. Fisher's interests were reviewed and are managed by
1079 Massachusetts General Hospital and Partners Healthcare in accordance with
1080 their conflict of interest policies.

1081 **Data and materials availability:** RNA-seq data have been deposited in the
1082 NCBI GEO database with accession number GSEXXXXX. Additional data that
1083 support the findings of this study are available from the corresponding author
1084 upon request.

1085 **References**

1086 1. Flavahan WA, Gaskell E, Bernstein BE. Epigenetic plasticity and the hallmarks
1087 of cancer. Science. 2017;357:eaal2380.

1088 2. Kim KH, Roberts CWM. Targeting EZH2 in cancer. Nature Medicine.
1089 2016;22:128–34.

1090 3. Dillon SC, Zhang X, Trievel RC, Cheng X. The SET-domain protein superfamily:
1091 protein lysine methyltransferases. Genome Biol. 2005;6:227.

1092 4. Yap DB, Chu J, Berg T, Schapira M, Cheng S-WG, Moradian A, et al. Somatic
1093 mutations at EZH2 Y641 act dominantly through a mechanism of selectively
1094 altered PRC2 catalytic activity, to increase H3K27 trimethylation. Blood.
1095 2011;117:2451–9.

1096 5. Souroullas GP, Jeck WR, Parker JS, Simon JM, Liu J-Y, Paulk J, et al. An oncogenic
1097 *Ezh2* mutation induces tumors through global redistribution of histone 3 lysine
1098 27 trimethylation. Nature Medicine. 2016;22:632–40.

1099 6. Weirich S, Kudithipudi S, Jeltsch A. Somatic cancer mutations in the MLL1
1100 histone methyltransferase modulate its enzymatic activity and dependence on
1101 the WDR5/RBBP5/ASH2L complex. Molecular Oncology. 2017;11:373–87.

1102 7. Weirich S, Kudithipudi S, Kycia I, Jeltsch A. Somatic cancer mutations in the
1103 MLL3-SET domain alter the catalytic properties of the enzyme. Clinical
1104 Epigenetics [Internet]. 2015 [cited 2018 Mar 30];7. Available from:
1105 http://www.clinicalepigeneticsjournal.com/content/7/1/36

1106 8. Jaffe JD, Wang Y, Chan HM, Zhang J, Huether R, Kryukov GV, et al. Global
1107 chromatin profiling reveals *NSD2* mutations in pediatric acute lymphoblastic
1108 leukemia. Nature Genetics. 2013;45:1386–91.

1109 9. Shinkai Y, Tachibana M. H3K9 methyltransferase G9a and the related molecule
1110 GLP. Genes Dev. 2011;25:781–8.

1111 10. Tachibana M, Sugimoto K, Nozaki M, Ueda J, Ohta T, Ohki M, et al. G9a histone
1112 methyltransferase plays a dominant role in euchromatic histone H3 lysine 9
1113 methylation and is essential for early embryogenesis. Genes Dev.
1114 2002;16:1779–91.

1115 11. Barski A, Cuddapah S, Cui K, Roh T-Y, Schones DE, Wang Z, et al. High-
1116 Resolution Profiling of Histone Methylations in the Human Genome. Cell.
1117 2007;129:823–37.

1118 12. Wei L, Chiu DK-C, Tsang FH-C, Law C-T, Cheng CL-H, Au SL-K, et al. Histone
1119 methyltransferase G9a promotes liver cancer development by epigenetic

1120 silencing of tumor suppressor gene RARRES3. Journal of Hepatology.
1121 2017;67:758–69.

1122 13. Ding J, Li T, Wang X, Zhao E, Choi J-H, Yang L, et al. The Histone H3
1123 Methyltransferase G9A Epigenetically Activates the Serine-Glycine Synthesis
1124 Pathway to Sustain Cancer Cell Survival and Proliferation. Cell Metabolism.
1125 2013;18:896–907.

1126 14. Dong C, Wu Y, Yao J, Wang Y, Yu Y, Rychahou PG, et al. G9a interacts with Snail
1127 and is critical for Snail-mediated E-cadherin repression in human breast cancer
1128 [Internet]. 2012 [cited 2018 Mar 30]. Available from: https://www-jci-org.ezp-
1129 prod1.hul.harvard.edu/articles/view/57349/pdf

1130 15. Tu WB, Shiah Y-J, Lourenco C, Mullen PJ, Dingar D, Redel C, et al. MYC Interacts
1131 with the G9a Histone Methyltransferase to Drive Transcriptional Repression
1132 and Tumorigenesis. Cancer Cell. 2018;34:579-595.e8.

1133 16. Garraway LA, Widlund HR, Rubin MA, Getz G, Berger AJ, Ramaswamy S, et al.
1134 Integrative genomic analyses identify *MITF* as a lineage survival oncogene
1135 amplified in malignant melanoma. Nature. 2005;436:117–22.

1136 17. Ceol CJ, Houvras Y, Jane-Valbuena J, Bilodeau S, Orlando DA, Battisti V, et al. The
1137 histone methyltransferase SETDB1 is recurrently amplified in melanoma and
1138 accelerates its onset. Nature. 2011;471:513–7.

1139 18. Kim M, Gans JD, Nogueira C, Wang A, Paik J-H, Feng B, et al. Comparative
1140 Oncogenomics Identifies NEDD9 as a Melanoma Metastasis Gene. Cell.
1141 2006;125:1269–81.

1142 19. Tachibana M, Ueda J, Fukuda M, Takeda N, Ohta T, Iwanari H, et al. Histone
1143 methyltransferases G9a and GLP form heteromeric complexes and are both
1144 crucial for methylation of euchromatin at H3-K9. Genes Dev. 2005;19:815–26.

1145 20. Liu F, Barsyte-Lovejoy D, Li F, Xiong Y, Korboukh V, Huang X-P, et al. Discovery
1146 of an in vivo Chemical Probe of the Lysine Methyltransferases G9a and GLP.
1147 Journal of medicinal chemistry [Internet]. 2013 [cited 2018 Mar 30];56.
1148 Available from:
1149 https://phstwlp2.partners.org:2052/pmc/articles/PMC3880643/

1150 21. Yokoyama S, Woods SL, Boyle GM, Aoude LG, MacGregor S, Zismann V, et al. A
1151 novel recurrent mutation in *MITF* predisposes to familial and sporadic
1152 melanoma. Nature. 2011;480:99–103.

1153 22. Levy C, Khaled M, Fisher DE. MITF: master regulator of melanocyte
1154 development and melanoma oncogene. Trends in Molecular Medicine.
1155 2006;12:406–14.

1156 23. Sato S, Roberts K, Gambino G, Cook A, Kouzarides T, Goding CR. CBP/p300 as a
1157 co-factor for the Microphthalmia transcription factor. Oncogene.
1158 1997;14:3083–92.

1159 24. Takeda K, Yasumoto K, Takada R, Takada S, Watanabe K, Udono T, et al.
1160 Induction of Melanocyte-specific Microphthalmia-associated Transcription
1161 Factor by Wnt-3a. Journal of Biological Chemistry. 2000;275:14013–6.

1162 25. Dorsky RI, Raible DW, Moon RT. Direct regulation of nacre, a zebrafish MITF
1163 homolog required for pigment cell formation, by the Wnt pathway. Genes Dev.
1164 2000;14:158–62.

1165 26. Rimm DL, Caca K, Hu G, Harrison FB, Fearon ER. Frequent Nuclear/Cytoplasmic
1166 Localization of β-Catenin without Exon 3 Mutations in Malignant Melanoma.
1167 The American Journal of Pathology. 1999;154:325–9.

1168 27. Zhan T. Wnt signaling in cancer. 2017;13.

1169 28. Morris LGT, Kaufman AM, Gong Y, Ramaswami D, Walsh LA, Turcan Ş, et al.
1170 Recurrent somatic mutation of FAT1 in multiple human cancers leads to
1171 aberrant Wnt activation. Nature Genetics. 2013;45:253–61.

1172 29. Spranger S, Gajewski TF. Impact of oncogenic pathways on evasion of
1173 antitumour immune responses. Nature Reviews Cancer. 2018;18:139–47.

1174 30. Spranger S, Bao R, Gajewski TF. Melanoma-intrinsic β-catenin signalling
1175 prevents anti-tumour immunity. Nature. 2015;523:231–5.

1176 31. Moreno BH, Zaretsky JM, Garcia-Diaz A, Tsoi J, Parisi G, Robert L, et al.
1177 Response to programmed cell death-1 blockade in a murine melanoma
1178 syngeneic model requires costimulation, CD4, and CD8 T cells. Cancer Immunol
1179 Res. 2016;4:845–57.

1180 32. Ayers M, Lunceford J, Nebozhyn M, Murphy E, Loboda A, Kaufman DR, et al.
1181 IFN-γ–related mRNA profile predicts clinical response to PD-1 blockade. J Clin
1182 Invest. 2017;127:2930–40.

1183 33. Segovia C, José-Enériz ES, Munera-Maravilla E, Martínez-Fernández M, Garate L,
1184 Miranda E, et al. Inhibition of a G9a/DNMT network triggers immune-mediated
1185 bladder cancer regression. Nat Med. 2019;25:1073–81.

1186 34. Nsengimana J, Laye J, Filia A, O'Shea S, Muralidhar S, Poźniak J, et al. β-Catenin–
1187 mediated immune evasion pathway frequently operates in primary cutaneous
1188 melanomas. J Clin Invest. 2018;128:2048–63.

1189 35. Bindea G, Mlecnik B, Tosolini M, Kirilovsky A, Waldner M, Obenauf AC, et al.
1190 Spatiotemporal Dynamics of Intratumoral Immune Cells Reveal the Immune
1191 Landscape in Human Cancer. Immunity. 2013;39:782–95.

1192 36. Allen EMV, Miao D, Schilling B, Shukla SA, Blank C, Zimmer L, et al. Genomic
1193 correlates of response to CTLA-4 blockade in metastatic melanoma. Science.
1194 2015;350:207–11.

1195 37. Hugo W, Zaretsky JM, Sun L, Song C, Moreno BH, Hu-Lieskovan S, et al. Genomic
1196 and Transcriptomic Features of Response to Anti-PD-1 Therapy in Metastatic
1197 Melanoma. Cell. 2016;165:35–44.

1198 38. Riaz N, Havel JJ, Makarov V, Desrichard A, Urba WJ, Sims JS, et al. Tumor and
1199 Microenvironment Evolution during Immunotherapy with Nivolumab. Cell.
1200 2017;171:934-949.e16.

1201 39. Hodis E, Watson IR, Kryukov GV, Arold ST, Imielinski M, Theurillat J-P, et al. A
1202 Landscape of Driver Mutations in Melanoma. Cell. 2012;150:251–63.

1203 40. Yu Y, Schleich K, Yue B, Ji S, Lohneis P, Kemper K, et al. Targeting the
1204 Senescence-Overriding Cooperative Activity of Structurally Unrelated H3K9
1205 Demethylases in Melanoma. Cancer Cell. 2018;33:322-336.e8.

1206 41. Wu H, Min J, Lunin VV, Antoshenko T, Dombrovski L, Zeng H, et al. Structural
1207 Biology of Human H3K9 Methyltransferases. PLoS One [Internet]. 2010 [cited
1208 2018 Oct 21];5. Available from:
1209 https://www.ncbi.nlm.nih.gov/pmc/articles/PMC2797608/

1210 42. Jia D, Jurkowska RZ, Zhang X, Jeltsch A, Cheng X. Structure of Dnmt3a bound to
1211 Dnmt3L suggests a model for de novo DNA methylation. Nature.
1212 2007;449:248–51.

1213 43. Zingg D, Debbache J, Peña-Hernández R, Antunes AT, Schaefer SM, Cheng PF, et
1214 al. EZH2-Mediated Primary Cilium Deconstruction Drives Metastatic Melanoma
1215 Formation. Cancer Cell. 2018;34:69-84.e14.

1216 44. Akbani R, Akdemir KC, Aksoy BA, Albert M, Ally A, Amin SB, et al. Genomic
1217 Classification of Cutaneous Melanoma. Cell. 2015;161:1681–96.

1218 45. Carbone M, Yang H, Pass HI, Krausz T, Testa JR, Gaudino G. BAP1 and cancer.
1219 Nat Rev Cancer. 2013;13:153–9.

1220 46. LaFave LM, Béguelin W, Koche R, Teater M, Spitzer B, Chramiec A, et al. Loss of
1221 BAP1 function leads to EZH2-dependent transformation. Nat Med.
1222 2015;21:1344–9.

1223 47. Campagne A, Lee M-K, Zielinski D, Michaud A, Le Corre S, Dingli F, et al. BAP1
1224 complex promotes transcription by opposing PRC1-mediated H2A
1225 ubiquitylation. Nat Commun. 2019;10:348.

1226 48. He M, Chaurushiya MS, Webster JD, Kummerfeld S, Reja R, Chaudhuri S, et al.
1227 Intrinsic apoptosis shapes the tumor spectrum linked to inactivation of the
1228 deubiquitinase BAP. 2019;4.

1229 49. Sharma P, Hu-Lieskovan S, Wargo JA, Ribas A. Primary, Adaptive, and Acquired
1230 Resistance to Cancer Immunotherapy. Cell. 2017;168:707–23.

1231 50. Damsky WE, Curley DP, Santhanakrishnan M, Rosenbaum LE, Platt JT,
1232 Gould Rothberg BE, et al. β-Catenin Signaling Controls Metastasis in Braf-
1233 Activated Pten-Deficient Melanomas. Cancer Cell. 2011;20:741–54.

1234 51. Sinnberg T, Makino E, Krueger MA, Velic A, Macek B, Rothbauer U, et al. A
1235 Nexus Consisting of Beta-Catenin and Stat3 Attenuates BRAF Inhibitor Efficacy
1236 and Mediates Acquired Resistance to Vemurafenib. EBioMedicine. 2016;8:132–
1237 49.

1238 52. Gartner JJ, Parker SCJ, Prickett TD, Dutton-Regester K, Stitzel ML, Lin JC, et al.
1239 Whole-genome sequencing identifies a recurrent functional synonymous
1240 mutation in melanoma. Proc Natl Acad Sci U S A. 2013;110:13481–6.

1241 53. Haq R, Shoag J, Andreu-Perez P, Yokoyama S, Edelman H, Rowe GC, et al.
1242 Oncogenic BRAF Regulates Oxidative Metabolism via PGC1α and MITF. Cancer
1243 Cell. 2013;23:302–15.

1244 54. Barbie DA, Tamayo P, Boehm JS, Kim SY, Moody SE, Dunn IF, et al. Systematic
1245 RNA interference reveals that oncogenic KRAS-driven cancers require TBK1.
1246 Nature. 2009;462:108–12.

1247 55. Li J, Song JS, Bell RJA, Tran T-NT, Haq R, Liu H, et al. YY1 Regulates Melanocyte
1248 Development and Function by Cooperating with MITF. Bosenberg M, editor.
1249 PLoS Genetics. 2012;8:e1002688.

1250 56. Newton-Bishop JA, Beswick S, Randerson-Moor J, Chang Y-M, Affleck P, Elliott F,
1251 et al. Serum 25-Hydroxyvitamin D3 Levels Are Associated With Breslow
1252 Thickness at Presentation and Survival From Melanoma. J Clin Oncol.
1253 2009;27:5439–44.

1254 57. Newton-Bishop JA, Davies JR, Latheef F, Randerson-Moor J, Chan M, Gascoyne J,
1255 et al. 25-hydroxyvitamin D2/D3 levels and factors associated with systemic
1256 inflammation and melanoma survival in the Leeds Melanoma Cohort. Int J
1257 Cancer. 2015;136:2890–9.

58. Scheinin I, Sie D, Bengtsson H, Wiel MA van de, Olshen AB, Thuijl HF van, et al. DNA copy number analysis of fresh and formalin-fixed specimens by shallow whole-genome sequencing with identification and exclusion of problematic regions in the genome assembly. Genome Res. 2014;24:2022–32.

1263 **Figure Legends**

1264

1265 **Figure 1. G9a recurrent mutations G1069L/W enhance catalytic activity and**
1266 **melanomagenesis.**

1267 **(A)** Domain architecture of human G9a and mutations reported in 16 publicly
1268 available whole exome sequence datasets of patient-derived melanomas (2034
1269 cases). Red arrowheads indicate recurrent nonsynonumous mutations. **(B)**
1270 Alignment of a portion of the human G9a SET domain with 8 different SET
1271 domain-containing histone methyltransferases. The blue and red columns
1272 indicate the highly conserved catalytic site tyrosine (e.g., EZH2 Y641 or G9a
1273 Y1067) and glycine (e.g., G9a G1069 or EZH2 G643), respectively. **(C)** GISTIC
1274 analysis (see Methods) revealed significant regions of recurrent focal
1275 chromosomal copy number gain/amplification among TCGA human melanomas.
1276 **(D)** *In vitro* methyltransferase assay using recombinant human G9a wild type
1277 (WT) and mutants in the presence or absence of recombinant GLP protein with
1278 different substrates: recombinant H3 protein, native human nucleosome,
1279 unmodified H3 tail peptide (1-16), monomethylated H3K9 (H3K9me1) peptide,
1280 and dimethylated H3K9 (H3K9me2) peptide. Data represent mean ± SD (n=4,
1281 representative of two independent experiments). **(E and F)** Representative
1282 images of soft agar culture (E) and colony numbers (F, top) and western blots (F,
1283 bottom) of pMEL* (left lane) and pMEL* transduced with $NRAS^{Q61R}$ and either
1284 GFP, G9a WT, G9a G1069L, or G9a G1069W. Data with error bars represent
1285 mean ± SD of 3-4 replicates from a representative of 3 independent experiments.

1286 Western blots show expression of V5-tagged G9a WT and mutants, as well as
1287 total- and phospho-ERK1/2, a downstream target of NRAS. **(G)** Kaplan-Meier
1288 plot showing melanoma-free survival of *BRAF*^{V600E};*tp53*$^{-/-}$ zebrafish injected with
1289 G9a G1069 mutant (pink and green) or EGFP (control, black) miniCoopR
1290 constructs. P-values were calculated by the log-rank (Mantel-Cox) test. The
1291 experiments were repeated twice independently by two different operator, and a
1292 representative cohort is shown. **(H)** Representative images of the zebrafish
1293 injected with EGFP, G9a WT, G9a G1069L, or G1069W miniCoopR. P-values
1294 were calculated by one-way ANOVA with the Holm-Šidák correction for multiple
1295 pairwise comparisons (**D** and **F**). *p<0.05, ***p<0.001, ****p<0.0001.
1296

1297 **Figure 2. G9a is required for growth in *G9a* copy number-gained melanoma**
1298 **cells.**

1299 **(A)** Proportions of TCGA melanomas with different *G9a* copy numbers. **(B)**
1300 Representative western blot of H3K9me2 in melanoma cell lines and primary
1301 human melanocytes. The numbers indicate qPCR-determined *G9a* copy
1302 numbers in *G9a*-gained/amplified (red) and -unamplified (black) melanoma lines
1303 and melanocytes; ND, not determined). The experiment was repeated four times
1304 independently (refer to Supplementary Fig. S3F). **(C)** Colony formation of *G9a*-
1305 gained or -amplified/H3K9me2-high and H3K9me2-low melanoma cell lines with
1306 *G9a* knockdown or control shRNA (shLuc). Data represent mean +/– SD of
1307 triplicates. P-values were calculated by one-way ANOVA with the Holm-Šidák
1308 correction for multiple pairwise comparisons. *p<0.05, **p<0.01, ****p<0.0001 vs.

1309 shLuc. **(D)** Dose-dependent growth inhibition by UNC0638 in melanoma cell lines
1310 and primary human melanocytes. Data represent mean +/– SD of triplicates from
1311 at least two independent experiments. **(E)** Western blotting for autophagy marker
1312 LC3B in *G9a*-gained melanoma cell lines WM983B and K029, and *G9a*-
1313 unamplified melanoma cell line UACC62. Cells were treated with UNC0638 at
1314 the indicated concentrations for 72h. Representative images from two-
1315 independent experiments were shown. **(F)** *In vivo* effect of potent G9a/GLP
1316 inhibitor UNC0642 (2.5 mg/kg) on growth of xenografts from *G9a*-
1317 gained/H3K9me2-high melanoma cell line K029. *$p<0.05$, ***$p<0.001$ by
1318 repeated measures two-way ANOVA with the Holm-Šidák correction for multiple
1319 pairwise comparisons of the two groups at each time point. N=5/group. **(G)**
1320 Representative immunohistochemistry images (40X) of H3K9me2 (top) and
1321 LC3B (bottom) in K029 melanoma xenograft tissue samples from mice treated
1322 with vehicle or UNC0642. **(H)** Growth of individual WM983B xenograft tumors in
1323 mice treated daily with vehicle (10% DMSO/PBS) (left, n=9) or UNC0642 (2.5
1324 mg/kg) (right, n=10). Red lines (2/10) indicate complete tumor regressions. **(I)**
1325 Kaplan-Meier survival curves of WM983B-xenografted mice treated with vehicle
1326 or UNC0642 (2.5 mg/kg). **$p<0.01$ by the log-rank (Mantel-Cox) test.

1327 **Figure 3. G9a stimulates MITF expression in melanoma through canonical**
1328 **WNT/β-catenin signaling.**

1329 **(A)** Volcano plot showing genes that are significantly altered by *G9a* knockdown
1330 in *G9a*-amplified Hs944T cells. The one red and six black dots indicate MITF and
1331 several of its target genes. The whole transcriptome RNA-seq was performed in

1332 duplicate. **(B)** qRT-PCR for MITF-M upon *G9a* knockdown in *G9a*-amplified, -
1333 gained, and *G9a* diploid melanoma cells. Data represent mean +/– SD of
1334 triplicates. *p<0.05, **p<0.01, ***p<0.001, ****p<0.0001 vs. shScr in the same cell
1335 line by two-way ANOVA with the Holm-Šidák correction for pairwise
1336 comparisons. (See also Supplementary Fig. S4, A-C) **(C and D)** Western blots of
1337 MITF and H3K9me2 72h after (C) *G9a* knockdown and (D) pharmacological
1338 inhibition in *G9a*-amplified (Hs944T) or -gained (WM983B and K029) melanoma
1339 cells. Representative images from at least two independent experiments are
1340 shown. **(E)** Rescue of *G9a*-amplified or gained melanoma cells from *G9a*
1341 knockdown by ectopic MITF overexpression. ****p<0.0001 by two-way ANOVA
1342 after normalizing to eliminate the difference between the shScr groups, with the
1343 Holm-Šidák correction for multiple pairwise comparisons. The data represent
1344 mean +/– SD from triplicates. **(F)** TOP/FOPFlash transcriptional activity 72 h after
1345 *G9a* knockdown in *G9a*-gained K029 melanoma cells. FOPFlash is a control
1346 luciferase reporter with mutant TCF/LEF-binding sites. Data represent mean +/–
1347 SD of 3-4 replicates from three independent experiments. **(G)** Western blots of
1348 MITF and non-phosphorylated (active) β-catenin in *G9a*-gained WM983B
1349 melanoma cells expressing constitutively active β-catenin (S33A) or empty
1350 vector, following incubation with UNC0638 (750 nM) for 72h. P-values were
1351 calculated by one-way ANOVA with the Holm-Šidák correction for multiple
1352 pairwise comparisons.
1353

1354 **Figure 4. G9a stimulates WNT/β-catenin and subsequent MITF expression**
1355 **by repressing WNT antagonist DKK1 in melanoma.**
1356 **(A)** Venn diagram shows genes that are downregulated by G9a overexpression
1357 in pMEL*/BRAF and upregulated by *G9a* knockdown in Hs944T, respectively
1358 (adjusted p-value<0.05). The 41 candidate target genes that overlap in the two
1359 datasets are shown in the box. **(B)** Snapshot image of G9a ChIP-seq peak in
1360 colon cancer initiating cells (GSE82131) at the putative DKK1 promoter region
1361 (from GENCODE). The publicly available dataset was visualized by IGV
1362 (ver_2.3.55). Green arrows indicate the primer set used for ChIP-qPCR in
1363 subsequent Figures 4C and 4D. **(C)** G9a ChIP-qPCR for DKK1 promoter in
1364 Hs944T and UACC62 cells. RPL30 (human RPL30 gene body (exon 3)) serves
1365 as a negative control. (n=3 from two independent experiments). **(D)** ChIP-qPCR
1366 of (left) H3K9me2 and (right) phosphorylated-RNA-polymerase II (pSer5) at the
1367 DKK1 promoter region in Hs944T cells. Cells were treated with DMSO or
1368 UNC0638 (500 nM) for 72 h and subjected to H3K9me2-ChIP or Pol II (pSer5)-
1369 ChIP. (n=3-4 from two independent experiments). **(E)** ELISA for secreted DKK1
1370 levels after UNC0638 (500 nM) for 72 h in *G9a*-amplified (Hs944T), -gained
1371 (WM983B and K029), and *G9a* diploid (UACC62) melanoma cells. Data
1372 represent mean +/– SD of 3-4 replicates. **(F)** Western blots of cytosolic and
1373 nuclear β-catenin and MITF expression in UNC0638-treated WM983B-shLuc and
1374 -shDKK1 cells. α-tubulin and LaminA/C served as internal controls for the
1375 cytosolic and nuclear fractions, respectively. Representative images from one of
1376 two independent experiments are shown. **(G and H)** Growth measured by

1377 CellTiter-Glo assay (n=4) (G) and western blot of autophagy marker LC3B
1378 (representative images from one of two independent experiments are shown) (H)
1379 in WM983B and K029 cells stably expressing shLuc or shDKK1 hairpins, after
1380 750 nM UNC0638 treatment for 72 h. P-values were calculated by unpaired, two-
1381 tailed T tests with the Holm-Šidák correction for multiple comparisons (**C**, **D** and
1382 **E**) or by two-way ANOVA with the Holm-Šidák correction for multiple pairwise
1383 comparisons (**G**). *p<0.05, ***p<0.001, ****p<0.0001.
1384
1385 **Figure 5. G9a-DKK1-WNT pathway is highly conserved across cancers and**
1386 **associated with a 'cold' tumor immune microenvironment.**
1387 **(A)** Correlations between mRNA expression levels of G9a and DKK1 in the
1388 indicated CCLE cancer cell line datasets. Each dot indicates one cell line in the
1389 dataset. **(B)** GSEA showing correlations between *G9a* expression and the WNT
1390 target gene set SANSOM_APC_TARGETS_REQUIRE_MYC (from MSigDB), in
1391 the same CCLE datasets as in (A). **(C)** Correlation between sensitivity to G9a
1392 inhibitor BIX-01294 (area-under-the-curve metric) and *G9a* mRNA level or copy
1393 number across cancers available in the CTRPv2 dataset. **(D)** Hierarchical
1394 clustering of 367 TCGA melanoma patients with average linkage by *G9a* copy
1395 number/expression and Spranger T-cell signature genes. Correlations between
1396 *G9a* expression and each T-cell signature gene were analyzed by Spearman's
1397 rank correlation. **(E and F)** Kaplan-Meier plots showing overall survival of mice
1398 harboring D4M.3A.3-UV3 tumors and treated with vehicle (n=6; gray dotted line),
1399 UNC0642 (5 mg/kg) (n=6; gray dashed line), anti-PD-1 (F) or anti-CTLA-4 (G)

1400 (n=6; gray dashed line), or combination therapy (UNC0642 + either anti-PD-1 or
1401 anti-CTLA-4) (n=8; black solid line). P-values were calculated by the log-rank
1402 (Mantel-Cox) test.

Figure 1.

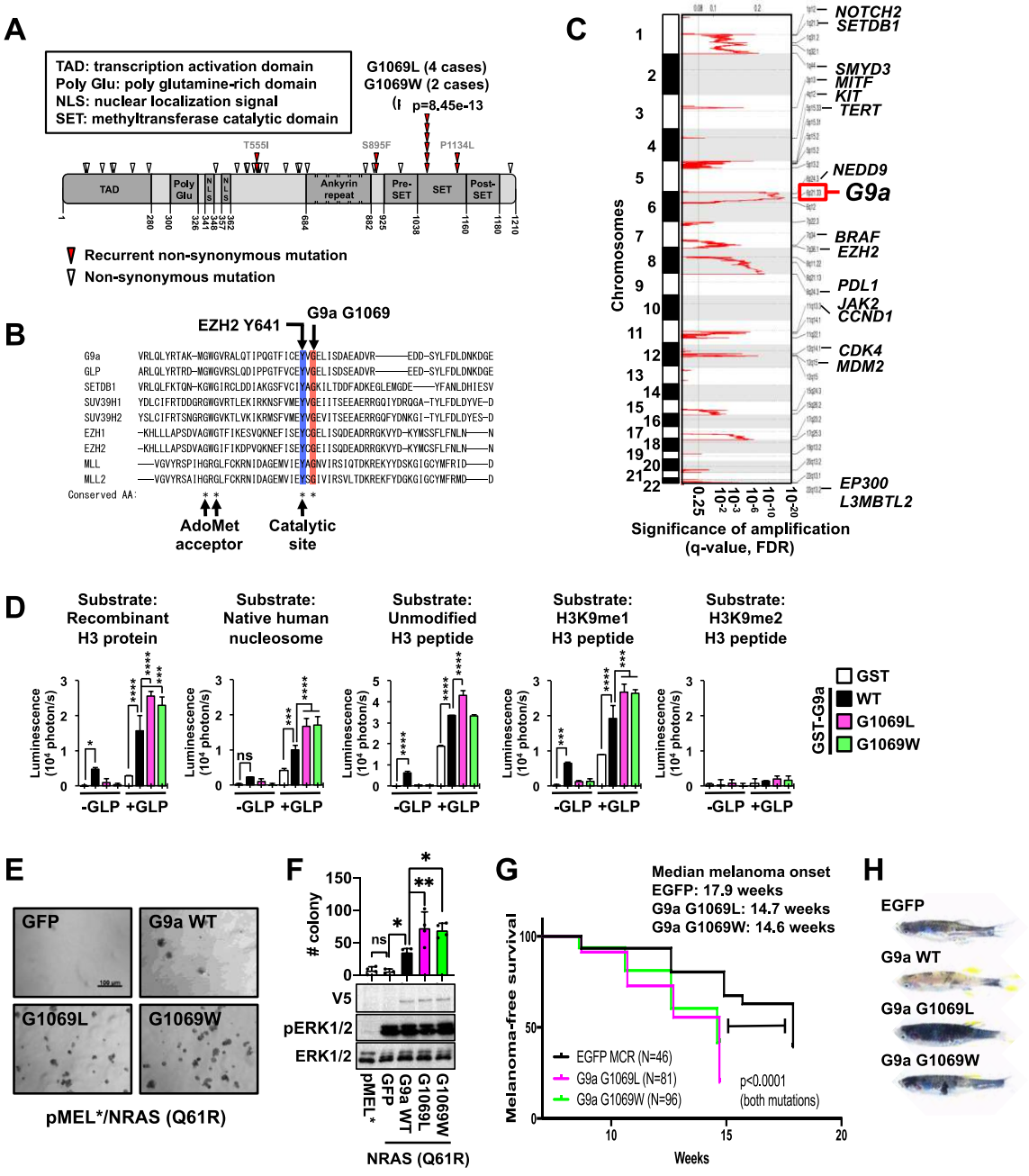
A
TAD: transcription activation domain
Poly Glu: poly glutamine-rich domain
NLS: nuclear localization signal
SET: methyltransferase catalytic domain
G1069L (4 cases)
G1069W (2 cases)
p=8.45e-13
T555I
S895F
P1134L
TAD
Poly Glu
NLS
Ankyrin repeat
Pre-SET
SET
Post-SET
Recurrent non-synonymous mutation
Non-synonymous mutation
B
EZH2 Y641
G9a G1069
AdoMet acceptor
Catalytic site
C
Chromosomes
NOTCH2
SETDB1
SMYD3
MITF
KIT
TERT
NEDD9
G9a
BRAF
EZH2
PDL1
JAK2
CCND1
CDK4
MDM2
EP300
L3MBTL2
Significance of amplification (q-value, FDR)
D
Substrate: Recombinant H3 protein
Substrate: Native human nucleosome
Substrate: Unmodified H3 peptide
Substrate: H3K9me1 H3 peptide
Substrate: H3K9me2 H3 peptide
Luminescence (10⁴ photon/s)
-GLP
+GLP
GST
WT
G1069L
G1069W
GST-G9a
E
GFP
G9a WT
G1069L
G1069W
pMEL*/NRAS (Q61R)
F
colony
V5
pERK1/2
ERK1/2
pMEL*
GFP
G9a WT
G1069L
G1069W
NRAS (Q61R)
G
Median melanoma onset
EGFP: 17.9 weeks
G9a G1069L: 14.7 weeks
G9a G1069W: 14.6 weeks
Melanoma-free survival
EGFP MCR (N=46)
G9a G1069L (N=81)
G9a G1069W (N=96)
p<0.0001
(both mutations)
Weeks
H
EGFP
G9a WT
G9a G1069L
G9a G1069W

Figure 2.

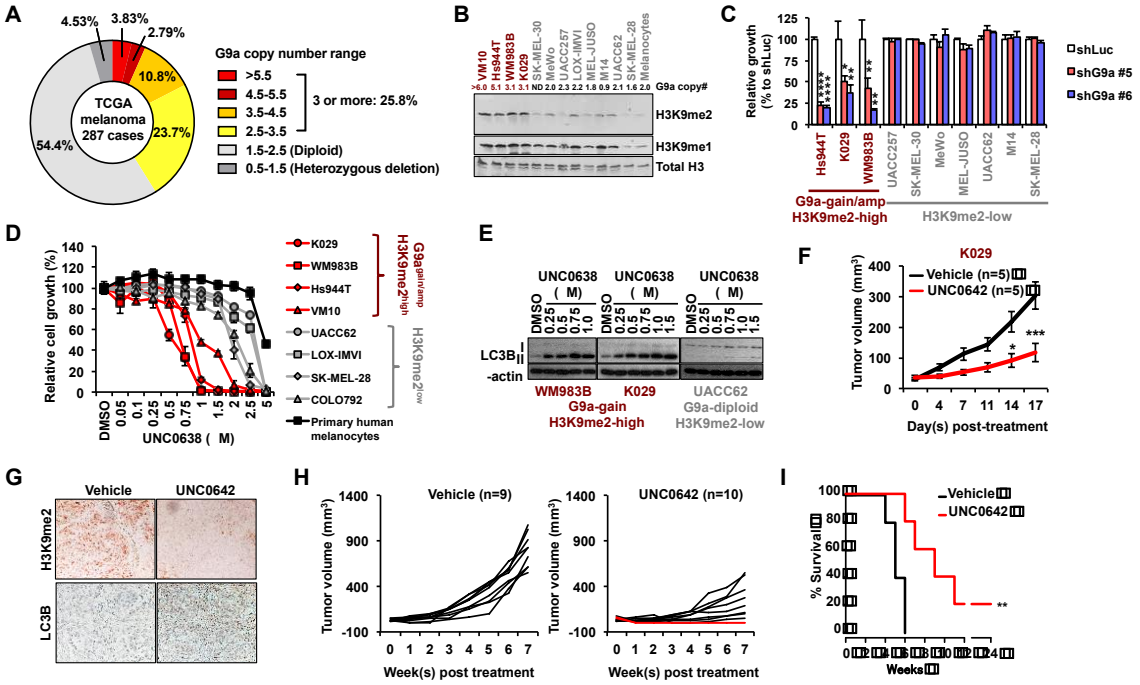
A
4.53%
3.83%
2.79%
10.8%
23.7%
54.4%
TCGA melanoma 287 cases
G9a copy number range
>5.5
4.5-5.5
3.5-4.5
2.5-3.5
3 or more: 25.8%
1.5-2.5 (Diploid)
0.5-1.5 (Heterozygous deletion)
B
VM10
Hs944T
WM983B
K029
SK-MEL-30
MeWo
UACC257
LOX-IMVI
MEL-JUSO
M14
UACC62
SK-MEL-28
Melanocytes
G9a copy#
H3K9me2
H3K9me1
Total H3
C
Relative growth (% to shLuc)
shLuc
shG9a #5
shG9a #6
G9a-gain/amp
H3K9me2-high
H3K9me2-low
D
Relative cell growth (%)
UNC0638 (M)
K029
WM983B
Hs944T
VM10
UACC62
LOX-IMVI
SK-MEL-28
COLO792
Primary human melanocytes
E
UNC0638 (M)
DMSO
LC3B
-actin
WM983B
K029
UACC62
G9a-gain
G9a-diploid
H3K9me2-high
H3K9me2-low
F
K029
Vehicle (n=5)
UNC0642 (n=5)
Tumor volume (mm³)
Day(s) post-treatment
G
Vehicle
UNC0642
H3K9me2
LC3B
H
Vehicle (n=9)
UNC0642 (n=10)
Tumor volume (mm³)
Week(s) post treatment
I
Vehicle
UNC0642
% Survival
Weeks

1408 **Figure 3.**

1409

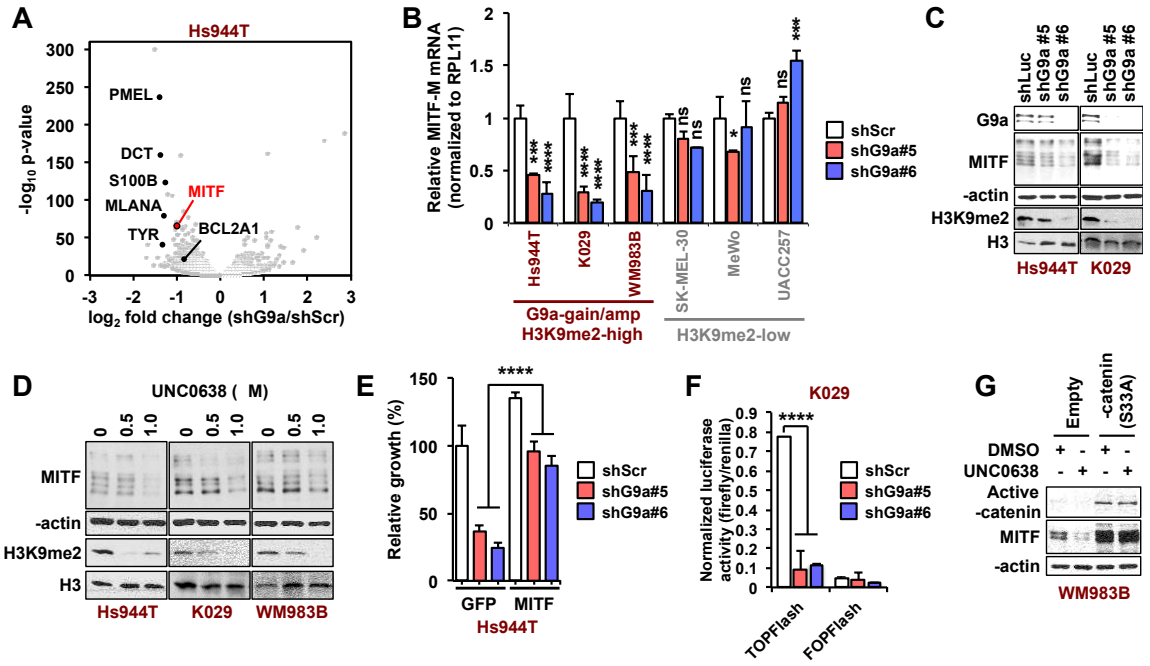

1410

1411

1412 **Figure 4.**

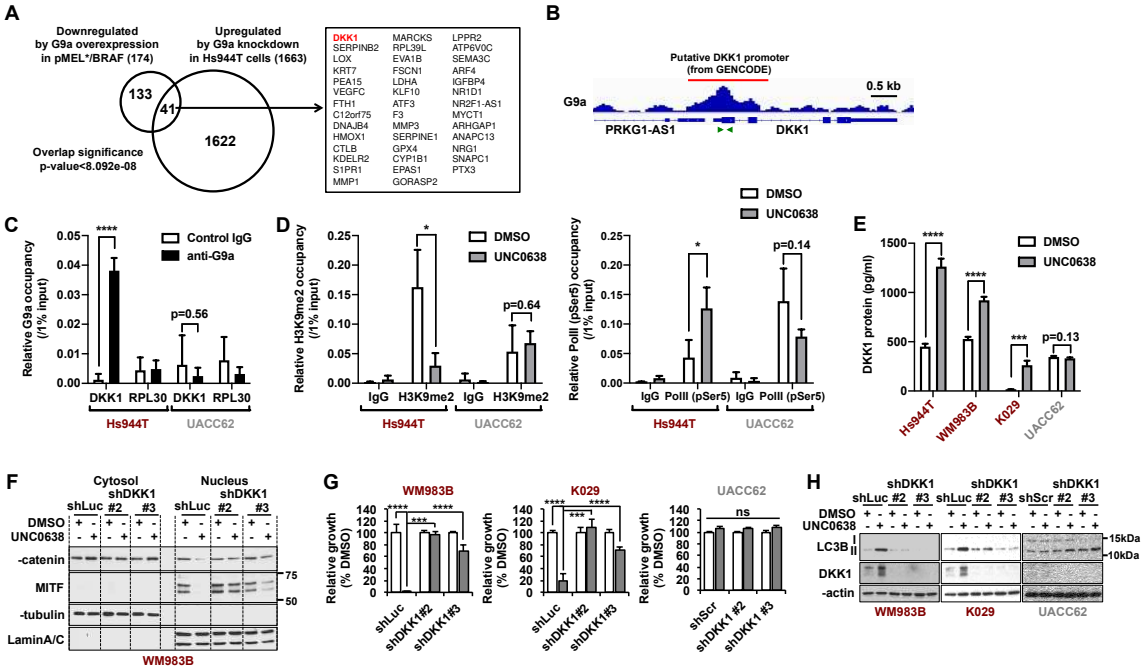

1413

Figure 5.

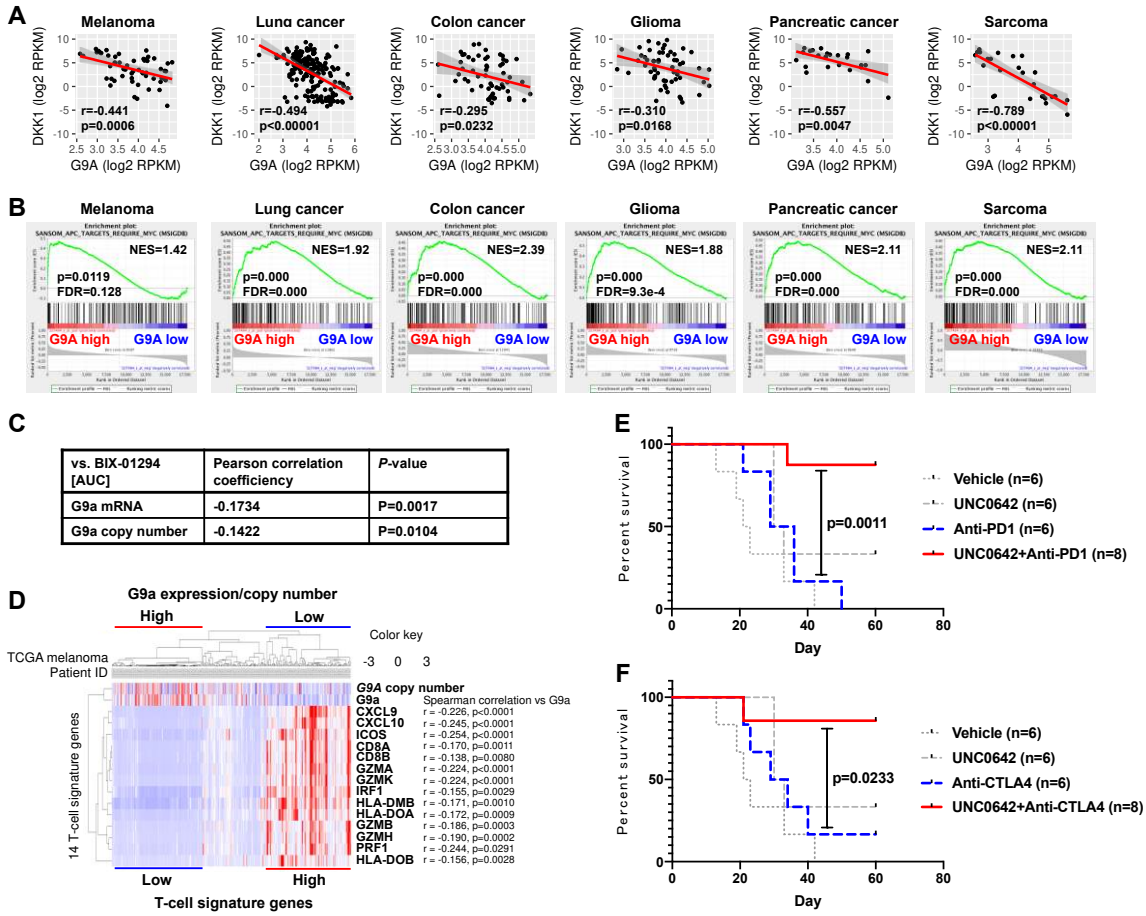

vs. BIX-01294 [AUC]	Pearson correlation coefficiency	*P*-value
G9a mRNA	-0.1734	P=0.0017
G9a copy number	-0.1422	P=0.0104